
MOX–Report No. 21/2013

# Coupled model and grid adaptivity in hierarchical reduction of elliptic problems

Perotto, S.; Veneziani, A.

MOX, Dipartimento di Matematica "F. Brioschi"
Politecnico di Milano, Via Bonardi 9 - 20133 Milano (Italy)

mox@mate.polimi.it http://mox.polimi.it

# Coupled model and grid adaptivity in hierarchical reduction of elliptic problems*

Simona Perotto[♯], Alessandro Veneziani[♭]

April 29, 2013

[♯] MOX– Modellistica e Calcolo Scientifico, Dipartimento di Matematica "F. Brioschi"
Politecnico di Milano, Piazza Leonardo da Vinci 32, I-20133 Milano, Italy
simona.perotto@polimi.it
[♭] Department of Mathematics and Computer Science, Emory University
400 Dowman Dr., 30322, Atlanta, GA, USA
ale@mathcs.emory.edu

**Keywords**: model reduction, a posteriori modeling error analysis, mesh adaptivity, domain decomposition, finite elements

**AMS Subject Classification**: 65N30, 65N15, 65T40

**Abstract**

In this paper we propose a *surrogate* model for advection-diffusion-reaction problems characterized by a dominant direction in their dynamics. We resort to a hierarchical-model reduction where we couple a modal representation of the transverse dynamics with a finite element approximation along the mainstream. This different treatment of the dynamics entails a surrogate model enhancing a purely 1D description related to the leading direction. The coefficients of the finite element expansion along this direction introduce a generally non-constant description of the transversal dynamics. Aim of this paper is to provide an automatic adaptive approach to locally select the dimension of the modal expansion as well as the finite element step in order to satisfy a prescribed tolerance on a goal functional of interest.

## 1 Introduction and motivations

In many applications involving an extensive use of scientific computing, a major problem is the identification of an appropriate trade-off between reliability

*This work has been partially supported by the PRIN 2010-2011 project "Innovative methods for water resources management under hydro-climatic uncertainty scenarios".

and computational cost of the numerical model. This leads in many cases to the identification of a *reduced* or *surrogate model* which is expected to be computationally affordable and mathematically reliable. As reference examples of surrogate models, we may cite the geometrical multiscale modeling of the circulatory system ([12, 9]), wavelet resolution of multiscale problems ([27]), pod methods applied, e.g., to nonlinear dynamical systems ([19]), compressed sensing ([11]). These model reduction procedures are somehow different and complementary to *surrogate solution* approaches based on the smart combination of off-line solutions of the full problem as, e.g., in a reduced basis approach ([24]).

In the proposal of an effective surrogate model one can take advantage of particular features of the problem at hand such as, for instance, a prevalent direction in the dynamics of interest. In this set, we include the design of networks, e.g., of pipes in internal combustion engines or in oil transportation, of channels when investigating waterways, of arteries in blood flow simulation. In all these applications, a standard approach consists in reducing the local dynamics in the single pipe to the axial component solely. Successively, the segments are connected via proper interface conditions. The main drawback of this approach is that local features of the investigated phenomena can be lost in the model reduction, yet they can be relevant for the global results. The presence of obstacles in an arterial district or in a hydrodynamic configuration, as well as the presence of an air filter in an internal combustion engine may require indeed a more precise model than the surrogate ones adopted for networks. For this reason, different options have been proposed, coupling a sharp local description with a global model. In this respect, it is worth recalling the coupling of dimensionally heterogeneous models advocated in [17] and [26] for describing interactions at different scales in hemodynamics and in river dynamics, respectively. Other approaches preserve the surrogate structure of the network model and introduce modifications to account for transverse dynamics of interest triggered by local features. In [33], for instance, the effect of the curvature of arteries is included in a "psychologically" one-dimensional model of blood flow by resorting to the so-called Cosserat director theory.

In a different way - yet with the same perspective of improving axial models rather than replacing them with dimensionally heterogeneous ones - in [16, 31] we have introduced a *hierarchical model* (hereafter shortened in Hi-Mod) *reduction* procedure, where we perform a modal approximation of the transverse dynamics coupled with a finite element discretization along the axial direction, in the spirit of a separation of variables. The rationale behind this idea is that the transverse dynamics can be suitably described with a few degrees of (modal) freedom, resulting in an *enriched* one-dimensional model. This is expected to improve the global reliability of a pure 1D model where we got rid of the transverse dynamics. An additional important feature of this approach is that the selection of the number $m$ of transverse modes can vary along the axis of the domain. Thus, by properly tuning $m$ over different regions of the computational domain, we are able to capture the local significant features of the solution with a relatively low

number of degrees of freedom.

The main purpose of this work is to make the local selection of the transverse modes automatic by introducing a *model adaptive procedure*. For this purpose, we derive an *a posteriori* modeling error estimator. In particular, we rely upon a goal-oriented approach, where the model prediction is driven by a goal functional representing a physical quantity of interest. We exploit the hierarchical structure characterizing the Hi-Mod approach in the a posteriori analysis as well. In the second part of the paper we extend the model adaptivity via an adaptive selection of the finite element partition to properly match possible local significant variations of the dynamics along the mainstream.
The analysis presented here refers to steady two-dimensional linear advection-diffusion-reaction problems and to linear goal functionals.

The paper is organized as follows. In Sect.2 we provide the geometric and functional basic ingredients for a Hi-Mod reduction. Section 3 provides the modeling error analysis, the corresponding model adaptive procedure and a numerical assessment. In Sect. 4 we merge the model with the mesh adaptation by deriving an *a posteriori* error estimator for the global error; an automatic procedure to select both the model and the mesh is consequently proposed and then validated on two test cases. Finally some perspectives are proposed in Sect. 5.

## 2 The hierarchical model reduction

Throughout the paper we refer to the following problem (weak form)

$$\text{find } u \in V \subseteq H^1(\Omega) \;\; \text{s.t.} \;\; a(u,v) = \mathcal{F}(v) \quad \forall v \in V, \tag{1}$$

as to the *full problem*, where $V$ is a suitable Hilbert space, $a(\cdot,\cdot)$ is a bilinear continuous and coercive form on $V \times V$ and $\mathcal{F}(\cdot)$ is a linear continuous functional on $V$. A standard notation is here adopted for the Sobolev spaces, as well as for the space of the functions bounded almost everywhere in $\Omega$ (see, e.g., [23]).

### 2.1 The geometric setting

We introduce the geometric constraints required to accomplish a Hi-Mod reduction (for more details we refer to [16, 31]).
We assume that the domain $\Omega \subset \mathbb{R}^d$, with $d \in \{2,3\}$, coincides with a $d$-dimensional fiber bundle, i.e., $\Omega = \bigcup_{x\in\Omega_{1D}} \{x\} \times \gamma_x$, where $\Omega_{1D}$ is the *supporting domain* described by only one independent variable $x$, while $\gamma_x \subset \mathbb{R}^{d-1}$ is the *tranverse fiber*, which is in general a function of $x$. In particular, we align $\Omega_{1D}$ with the main dynamic exhibited by the problem at hand, while the fibers $\gamma_x$ are associated with the secondary transverse dynamics. For the sake of simplicity, we choose $\Omega_{1D}$ as the interval $]x_0, x_1[$, the extension to curved domains being however feasible (see [30]). The boundary $\partial\Omega$ of $\Omega$ is split into three parts, i.e., $\partial\Omega = \Gamma_0 \cup \Gamma_1 \cup \Gamma^*$, being $\Gamma_i = \{x_i\} \times \gamma_{x_i}$ with $i \in \{0,1\}$, and $\Gamma_* = \bigcup_{x\in\Omega_{1D}} \partial\gamma_x$.

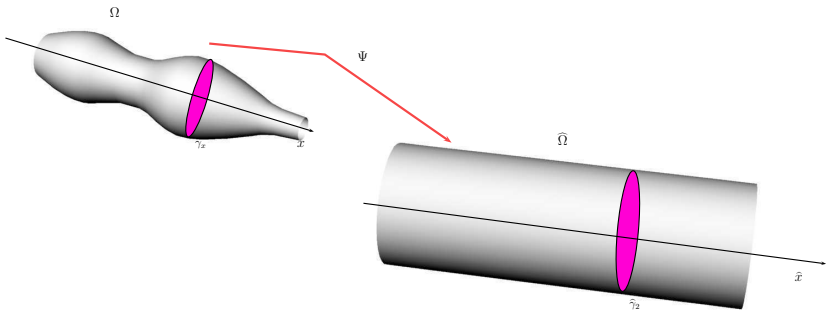


Figure 1: Example of the map $\Psi$ in a 3D framework

We assume that either homogeneous Dirichlet or homogeneous Neumann boundary conditions can be enforced on $\Gamma_0$, $\Gamma_1$ and $\Gamma_*$, as well as non-homogeneous Dirichlet data can be assigned on $\Gamma_0$ and $\Gamma_1$.

We introduce the map $\psi_x : \gamma_x \to \widehat{\gamma}_{d-1}$ between the fiber $\gamma_x$ and a reference fiber $\widehat{\gamma}_{d-1} \subset \mathbb{R}^{d-1}$. This application induces in turn the general map $\Psi : \Omega \to \widehat{\Omega}$ between the physical domain $\Omega$ and the reference domain $\widehat{\Omega} \equiv \bigcup_{x\in\Omega_{1D}} \{x\}\times\widehat{\gamma}_{d-1}$. Thus a generic point in $\Omega$ ($\widehat{\Omega}$) is referred to as $\boldsymbol{\zeta} = (x, \mathbf{y})(\widehat{\boldsymbol{\zeta}} = \Psi(\boldsymbol{\zeta}) = (\widehat{x}, \widehat{\mathbf{y}})$, with $\widehat{x} = x$ and $\widehat{\mathbf{y}} = \psi_x(\mathbf{y})$). Without loss of generality, we assume $\Omega_{1D}$ to be the subset of $\Omega$ with $\mathbf{y} = \mathbf{0}$, i.e., $\Omega_{1D}$ coincides with the centerline of the domain. In 2D, $\psi_x$ coincides with the linear transformation

$$\widehat{y} = \psi_x(y) = \frac{y}{L(x)}, \tag{2}$$

with $L(x) = \text{meas}(\gamma_x)$. We postulate regularity for both $\psi_x$ and $\Psi$: for all $x \in \Omega_{1D}$, $\psi_x$ is a $C^1-$diffeomorphism and $\Psi$ is differentiable with respect to $\boldsymbol{\zeta}$. This essentially excludes the presence of kinks along $\Gamma_*$.
In Figure 1 we sketch the main geometric quantities involved in the Hi-Mod reduction for $d = 3$.

## 2.2 The piecewise Hi-Mod reduction

We exploit the fiber structure introduced on $\Omega$ to fix the reduced formulation. As pointed out in Section 1, the axial prevalent dynamics will be spanned by one-dimensional $H^1$-functions, while the transverse dynamics are expanded in terms of a modal basis.

We introduce a number of definitions needed by the piecewise Hi-Mod framework. We first introduce a $d$-dimensional partition $\mathcal{T}_\Omega = \{\Omega_i\}_{i=1}^s$ of $\Omega$ into $s$ subdomains $\Omega_i = \bigcup_{x\in\Omega_{1D,i}} \{x\} \times \gamma_x$, with $\Omega_{1D,i} = (\sigma_{i-1}, \sigma_i)$ the generic subinterval of $\Omega_{1D}$ such that $\sigma_0 \equiv x_0$, $\sigma_s \equiv x_1$, $\cup_{i=1}^s \overline{\Omega}_{1D,i} = \overline{\Omega}_{1D}$, $\Omega_{1D,i} \cap \Omega_{1D,\tilde{i}} = \emptyset$ for $i \neq \tilde{i}$ and $i, \tilde{i} \in \{1, \dots, s\}$, and where we denote with $\Sigma_j = \{\sigma_j\} \times \gamma_{\sigma_j}$ the interface between $\Omega_j$ and $\Omega_{j+1}$, for $j \in \{1, \dots, s-1\}$ (see Figure 2 for an example).

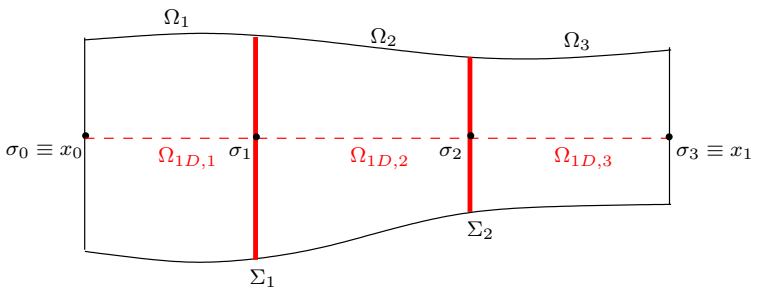


Figure 2: Example of 2D partition $\mathcal{T}_\Omega$ for $s = 3$

Let $H^1(\Omega, \mathcal{T}_\Omega)$ be the $d$-dimensional broken Sobolev space associated with the partition $\mathcal{T}_\Omega$, properly modified according to the boundary conditions assigned on $\partial\Omega$ ([22]); the trivial inclusion $V \subset H^1(\Omega, \mathcal{T}_\Omega)$ holds. Successively, we consider a *modal basis* of functions $\{\varphi_k\}_{k\in\mathbb{N}^+} \subseteq H^1(\widehat{\gamma}_{d-1})$, orthonormal with respect to the $L^2$-scalar product on $\widehat{\gamma}_{d-1}$ and compatible with the boundary conditions on $\Gamma_*$.

Finally, we introduce the *hierarchically reduced broken space*

$$
\begin{aligned}
V^b_{\mathbf{m}}(\mathcal{T}_\Omega) = \Big\{ v^b_{\mathbf{m}} \in L^2(\Omega) : v^b_{\mathbf{m}}|_{\Omega_i}(x,\mathbf{y}) = \sum_{k=1}^{m_i} v^i_k(x)\, \varphi_k(\psi_x(\mathbf{y}))\ \forall i \in \{1,\dots,s\}, \\
v^i_k \in H^1(\Omega_{1D,i})\ :\ \forall \tilde{k} \in \{1,\dots,m^j_\perp\} \text{ with } j \in \{1,\dots,s-1\}, \\
\int_{\widehat{\gamma}_{d-1}} \left(v^b_{\mathbf{m}}|_{\Omega_{j+1}}(\sigma_j, \psi^{-1}_{\sigma_j}(\widehat{\mathbf{y}})) - v^b_{\mathbf{m}}|_{\Omega_j}(\sigma_j, \psi^{-1}_{\sigma_j}(\widehat{\mathbf{y}}))\right) \varphi_{\tilde{k}}(\widehat{\mathbf{y}})\, d\widehat{\mathbf{y}} = 0 \Big\},
\end{aligned}
\tag{3}
$$

with $\mathbf{m} = \{m_i\}_{i=1}^s \in [\mathbb{N}^+]^s$ a given *modal multi-index*, $m^j_\perp = \min(m_j, m_{j+1})$. According to definition (3), a different number of modal basis functions can be employed in the subdomains $\Omega_i$: ideally, $m_i$ is large where the transverse dynamics are relevant, while it is small where these dynamics are less important. Thus, index $\mathbf{m}$ is piecewise constant. This explains the term *piecewise* Hi-Mod reduction in contrast to the *uniform* approach (see [16, 31]), where the same number of modal functions is employed on the whole $\Omega$.

Space $V^b_{\mathbf{m}}(\mathcal{T}_\Omega)$ is contained in $H^1(\Omega, \mathcal{T}_\Omega)$. In particular, let $m_{\min}$ be the minimum number of transverse modes over the entire domain. Then, the interface condition in (3) weakly enforces the continuity of the first $m_{\min}$ modes in the whole $\Omega$. Different strategies can be pursued to enforce this condition. In [31] we resort to an iterative substructuring Dirichlet/Neumann method (see, e.g., [32, 34]). Concerning the choice of the modal basis $\{\varphi_k\}_{k\in\mathbb{N}^+}$, several options are available. We have tested sinusoidal functions and Legendre polynomials.

The *piecewise hierarchically reduced* problem reads: given a modal multi-index $\mathbf{m} \in [\mathbb{N}^+]^s$, find $u^b_{\mathbf{m}} \in V^b_{\mathbf{m}}(\mathcal{T}_\Omega)$ s.t.

$$
a_{\mathcal{T}_\Omega}(u^b_{\mathbf{m}}, v^b_{\mathbf{m}}) = \mathcal{F}_{\mathcal{T}_\Omega}(v^b_{\mathbf{m}}) \quad \forall v^b_{\mathbf{m}} \in V^b_{\mathbf{m}}(\mathcal{T}_\Omega), \tag{4}
$$

with

$$a_{\mathcal{T}_\Omega}(u^b_{\mathbf{m}}, v^b_{\mathbf{m}}) = \sum_{i=1}^{s} a_i(u^b_{\mathbf{m}}|_{\Omega_i}, v^b_{\mathbf{m}}|_{\Omega_i}), \quad \mathcal{F}_{\mathcal{T}_\Omega}(v^b_{\mathbf{m}}) = \sum_{i=1}^{s} \mathcal{F}_i(v^b_{\mathbf{m}}|_{\Omega_i})$$

where $a_i(\cdot,\cdot)$ and $\mathcal{F}_i(\cdot)$ are the restrictions to the subdomain $\Omega_i$ of the bilinear and linear form in (1), respectively for $i \in \{1,\dots,s\}$. Formulation (4) is well-posed in $V^b_{\mathbf{m}}(\mathcal{T}_\Omega)$, with respect to the broken energy norm $\|v^b_{\mathbf{m}}\|_{\mathcal{T}_\Omega} = \left(\sum_{i=1}^{s} \|v^b_{\mathbf{m}}|_{\Omega_i}\|^2_{H^1(\Omega_i)}\right)^{1/2}$. The reduced solution $u^b_{\mathbf{m}}$ does not necessarily provide a $H^1$-conforming approximation to the full solution $u$ in (1): the continuity on $\Omega$ of both the trace and the flux of $u^b_{\mathbf{m}}$ is guaranteed to the first $m_{\min}$ modal components only. As proved in [31, Section 4.2.2], a conforming approximation is yielded only if $m_i > m_{i+1}$, for any $i \in \{1,\dots,s-1\}$.

**Remark 2.1** *The piecewise reduced formulation* (4) *admits, as a subcase, the uniform formulation introduced in [16, 31], when* $\mathbf{m}$ *has constant components.*

**Remark 2.2** *The broken space* $V^b_{\mathbf{m}}(\mathcal{T}_\Omega)$ *is similar to a mortar space. Here, the space spanned by the modal functions replaces the mortar trace space. In addition, all the matching conditions are weakly imposed in* (3)*; this is not the case for the mortar approach (see, e.g., [8, 21]).*

For the sake of numerical approximation, we introduce now the discrete counterpart of (4). We perform a finite element discretization (see, e.g., [13]) along $\Omega_{1D}$, while preserving the modal expansion along the transverse directions. We introduce the subdivision $\mathcal{T}^i_h$ of $\Omega_{1D,i}$ into the subintervals $K^i_l = (x^i_{l-1}, x^i_l)$ of width $h^i_l = x^i_l - x^i_{l-1}$ for $l \in \{1,\dots,n_i\}$, $i \in \{1,\dots,s\}$ and $n_i \in \mathbb{N}^+$. The hierarchically reduced *discrete* broken space is then given by

$$\begin{aligned} V^{b,h}_{\mathbf{m}}(\mathcal{T}_\Omega, \{\mathcal{T}^i_h\}) = \Big\{ v^{b,h}_{\mathbf{m}} \in V^b_{\mathbf{m}}(\mathcal{T}_\Omega) \ : \ v^{b,h}_{\mathbf{m}}|_{\Omega_i}(x,\mathbf{y}) = \sum_{k=1}^{m_i} v^{i,h}_k(x)\, \varphi_k(\psi_x(\mathbf{y})) \\ \forall i \in \{1,\dots,s\},\ v^{i,h}_k \in V^{i,h}_{1D} \Big\} \subset V^b_{\mathbf{m}}(\mathcal{T}_\Omega), \end{aligned} \tag{5}$$

where $V^{i,h}_{1D} \subset H^1(\Omega_{1D,i})$ is a finite element space associated with $\mathcal{T}^i_h$, such that $\dim(V^{i,h}_{1D}) = N^i_h < +\infty$. A density assumption is made on the spaces $V^{i,h}_{1D}$ ([13]). Thus the *piecewise hierarchically reduced discrete* problem reads: given a modal multi-index $\mathbf{m} \in [\mathbb{N}^+]^s$, find $u^{b,h}_{\mathbf{m}} \in V^{b,h}_{\mathbf{m}}(\mathcal{T}_\Omega, \{\mathcal{T}^i_h\})$ s.t.

$$a_{\mathcal{T}_\Omega}(u^{b,h}_{\mathbf{m}}, v^{b,h}_{\mathbf{m}}) = \mathcal{F}_{\mathcal{T}_\Omega}(v^{b,h}_{\mathbf{m}}) \quad \forall v^{b,h}_{\mathbf{m}} \in V^{b,h}_{\mathbf{m}}(\mathcal{T}_\Omega, \{\mathcal{T}^i_h\}). \tag{6}$$

The unknowns in (6) are the modal coefficients $u^{i,h}_k$ of $u^{b,h}_{\mathbf{m}}$, for $k \in \{1,\dots,m_i\}$ and $i \in \{1,\dots,s\}$ . From a computational viewpoint, we solve $s$ systems of coupled 1D problems. Each system is characterized by a sparse $m_i \times m_i$ block matrix and each $N^i_h \times N^i_h$ block exhibits the sparsity pattern typical of 1D finite

element approximations (tridiagonal for piecewise linear elements, pentadiagonal for piecewise quadratic elements, etc.)

By subtracting (6) from (4) for $v^b_{\mathbf{m}} = v^{b,h}_{\mathbf{m}}$, we get a standard Galerkin orthogonality property, i.e.,

$$a_{\mathcal{T}_\Omega}(\varepsilon^{b,h}_{\mathbf{m}}, v^{b,h}_{\mathbf{m}}) = 0 \quad \forall v^{b,h}_{\mathbf{m}} \in V^{b,h}_{\mathbf{m}}(\mathcal{T}_\Omega, \{\mathcal{T}^i_h\}), \tag{7}$$

where $\varepsilon^{b,h}_{\mathbf{m}} = u^b_{\mathbf{m}} - u^{b,h}_{\mathbf{m}}$ is the discretization error associated with the discrete formulation (6).

# 3 Automatic piecewise Hi-Mod reduction

Our aim is to devise an automatic procedure to select both the subdomains $\Omega_i$ and the modal multi-index $\mathbf{m}$ in (3). For this purpose, we propose an *a posteriori* modeling error estimator. In particular, we are interested in a*goal-oriented framework* where the accuracy of the adopted model is measured via a user-defined functional, which represents a physical quantity to be measured (e.g., mean or local values, convective or diffusive fluxes, the lift and drag coefficients around bodies in external flows, etc.).
Throughout this section we assume that the finite element partition associated with the broken space (5) is sufficiently fine to neglect the discretization error. This assumption will be removed in the next section.

## 3.1 A goal-oriented hierarchical modeling error estimator

Let $J : H^1(\Omega, \mathcal{T}_\Omega) \to \mathbb{R}$ be the output functional we are interested in. For simplicity, we assume a linear functional. We approximate the goal value $J(u)$ via $J(u^b_{\mathbf{m}})$, with $u$ and $u^b_{\mathbf{m}}$ solution to (1) and (4), respectively. Our purpose is to estimate the goal error $J(u - u^b_{\mathbf{m}})$ via a computable quantity, and, in particular, we aim at selecting the subdomains $\Omega_i$ and the modal multi-index $\mathbf{m}$ to keep the estimated error under a desired tolerance.

We introduce the piecewise hierarchically reduced dual problem associated with (4) and $J$: given a modal multi-index $\mathbf{m} \in [\mathbb{N}^+]^s$, find $z^b_{\mathbf{m}} \in V^b_{\mathbf{m}}(\mathcal{T}_\Omega)$ s.t.

$$a_{\mathcal{T}_\Omega}(v^b_{\mathbf{m}}, z^b_{\mathbf{m}}) = J(v^b_{\mathbf{m}}) \quad \forall v^b_{\mathbf{m}} \in V^b_{\mathbf{m}}(\mathcal{T}_\Omega), \tag{8}$$

where we mean $J(\cdot) = \sum_{i=1}^s J_i(\cdot)$, denoting by $J_i$ the restriction of $J$ to the subdomain $\Omega_i$, for $i \in \{1, \dots, s\}$.

Let $V^b_{\mathbf{m}^+}(\mathcal{T}_\Omega)$ be the *enriched* hierarchically reduced broken space, with $\mathbf{m}^+ \in [\mathbb{N}^+]^s$ such that $\mathbf{m}^+ > \mathbf{m}$, i.e., $m^+_i > m_i$, for any $i \in \{1, \dots, s\}$. The inclusions $V^b_{\mathbf{m}}(\mathcal{T}_\Omega) \subset V^b_{\mathbf{m}^+}(\mathcal{T}_\Omega) \subset H^1(\Omega, \mathcal{T}_\Omega)$ hold. On $V^b_{\mathbf{m}^+}(\mathcal{T}_\Omega)$ we define the *enriched* piecewise hierarchically reduced problem, find $u^b_{\mathbf{m}^+} \in V^b_{\mathbf{m}^+}(\mathcal{T}_\Omega)$ s.t.

$$a_{\mathcal{T}_\Omega}(u^b_{\mathbf{m}^+}, v^b_{\mathbf{m}^+}) = \mathcal{F}_{\mathcal{T}_\Omega}(v^b_{\mathbf{m}^+}) \quad \forall v^b_{\mathbf{m}^+} \in V^b_{\mathbf{m}^+}(\mathcal{T}_\Omega), \tag{9}$$

as well as the corresponding dual problem, find $z^b_{\mathbf{m}^+} \in V^b_{\mathbf{m}^+}(\mathcal{T}_\Omega)$ s.t.

$$a_{\mathcal{T}_\Omega}(v^b_{\mathbf{m}^+}, z^b_{\mathbf{m}^+}) = J(v^b_{\mathbf{m}^+}) \quad \forall v^b_{\mathbf{m}^+} \in V^b_{\mathbf{m}^+}(\mathcal{T}_\Omega). \tag{10}$$

Inclusion $V^b_{\mathbf{m}}(\mathcal{T}_\Omega) \subset V^b_{\mathbf{m}^+}(\mathcal{T}_\Omega)$ guarantees the orthogonality relations

$$a_{\mathcal{T}_\Omega}(u^b_{\mathbf{m}^+} - u^b_{\mathbf{m}}, v^b_{\mathbf{m}}) = 0, \quad a_{\mathcal{T}_\Omega}(v^b_{\mathbf{m}}, z^b_{\mathbf{m}^+} - z^b_{\mathbf{m}}) = 0 \quad \forall v^b_{\mathbf{m}} \in V^b_{\mathbf{m}}(\mathcal{T}_\Omega). \tag{11}$$

We can prove now the following preliminary result:

**Proposition 3.1** *For any* $\mathbf{m}$, $\mathbf{m}^+ \in [\mathbb{N}^+]^s$ *with* $\mathbf{m}^+ > \mathbf{m}$,

$$J(\delta u^b_{\mathbf{m}\mathbf{m}^+}) = a_{\mathcal{T}_\Omega}(\delta u^b_{\mathbf{m}\mathbf{m}^+}, \delta z^b_{\mathbf{m}\mathbf{m}^+}),$$

*with* $\delta u^b_{\mathbf{m}\mathbf{m}^+} = u^b_{\mathbf{m}^+} - u^b_{\mathbf{m}}$ *and* $\delta z^b_{\mathbf{m}\mathbf{m}^+} = z^b_{\mathbf{m}^+} - z^b_{\mathbf{m}}$.

**Proof.** We choose in (10) $v^b_{\mathbf{m}^+} = \delta u^b_{\mathbf{m}\mathbf{m}^+} \in V^b_{\mathbf{m}^+}(\mathcal{T}_\Omega)$ and then we exploit the orthogonality property $(11)_1$ with $v^b_{\mathbf{m}} = z^b_{\mathbf{m}} \in V^b_{\mathbf{m}}(\mathcal{T}_\Omega)$, to get

$$J(\delta u^b_{\mathbf{m}\mathbf{m}^+}) = a_{\mathcal{T}_\Omega}(\delta u^b_{\mathbf{m}\mathbf{m}^+}, z^b_{\mathbf{m}^+}) = a_{\mathcal{T}_\Omega}(\delta u^b_{\mathbf{m}\mathbf{m}^+}, \delta z^b_{\mathbf{m}\mathbf{m}^+}).$$

□

Should we assume that $u^b_{m^+}$ is a better approximation of $u^b_m$, we obtain a two-side bound for the functional modeling error.

**Proposition 3.2** *Let* $e^b_{\mathbf{m}} = u - u^b_{\mathbf{m}} \in H^1(\Omega, \mathcal{T}_\Omega)$ *be the* modeling error *associated with the reduced formulation* (4). *Correspondingly,* $e^b_{\mathbf{m}^+} = u - u^b_{\mathbf{m}^+}$ *is the enhanced error, belonging to the same space. Let us assume that there exists a positive constant* $\beta_{\mathbf{m}} < 1$ *and a modal multi-index* $\mathbf{M}_0 \in [\mathbb{N}^+]^s$, *such that, for* $\mathbf{m}, \mathbf{m}^+ \in [\mathbb{N}^+]^s$ *with* $\mathbf{m}^+ > \mathbf{m} \geq \mathbf{M}_0$,

$$|J(e^b_{\mathbf{m}^+})| \leq \beta_{\mathbf{m}} |J(e^b_{\mathbf{m}})|. \tag{12}$$

*Then,*

$$\frac{|J(\delta u^b_{\mathbf{m}\mathbf{m}^+})|}{1 + \beta_{\mathbf{m}}} \leq |J(e^b_{\mathbf{m}})| \leq \frac{|J(\delta u^b_{\mathbf{m}\mathbf{m}^+})|}{1 - \beta_{\mathbf{m}}}. \tag{13}$$

**Proof.** Result (13) is a straightforward consequence of the linearity of $J$, assumption (12) and the triangle inequality. □

Now relation (13) combined with Proposition 3.1 leads us to define the value

$$\eta^b_{\mathbf{m}\mathbf{m}^+} = |a_{\mathcal{T}_\Omega}(\delta u^b_{\mathbf{m}\mathbf{m}^+}, \delta z^b_{\mathbf{m}\mathbf{m}^+})|. \tag{14}$$

This is our *a posteriori* modeling error estimator for the functional modeling error $|J(e^b_{\mathbf{m}})|$: in particular, the lower and the upper bound in (13) represents the corresponding efficiency and a reliability estimate, respectively[1].

Estimator $\eta^b_{\mathbf{m}\mathbf{m}^+}$ is a goal-oriented hierarchical *a posteriori* modeling error estimator since it exhibits the typical structure of a hierarchical error estimator yet in a goal functional setting. This allows us to combine the easy computability typical of a hierarchical estimator with the high versatility proper of a goal functional analysis as far as concerns the quantity of interest.

[1]From (12)-(13), the further upper bound $|J(e^b_{\mathbf{m}^+})| \leq \beta_{\mathbf{m}}/(1 - \beta_{\mathbf{m}})\, |J(\delta u^b_{\mathbf{m}\mathbf{m}^+})|$ trivially descends.

**Remark 3.1** *Hypothesis* (12) *is a* saturation assumption. *This hypothesis is rather usual in a hierarchical framework: in [5, 15, 6, 1], for instance, this assumption is introduced in the context of an* a posteriori *analysis for the energy norm of the discretization error associated with a finite element approximation. Requirement* (12) *essentially generalizes a standard saturation hypothesis to the context of a modeling error analysis, by including the functional used to measure the error. This sounds reasonable in a goal-oriented framework. This assumption will be discussed further in Section 3.3 upon numerical evidence.*

### 3.2 The m-adaptive procedure

The **m**-adaptive procedure we aim at introducing is intended to provide the number and the location of the subdomains $\Omega_i$, together with the associated modal size $m_i$. To this aim, we suggest here a possible strategy based on the modeling error estimator (14).
To evaluate $\eta^b_{\mathbf{m}\mathbf{m}^+}$, we replace the piecewise hierarchically reduced primal and dual solutions with the discrete approximations $u^{b,h}_{\mathbf{m}}, z^{b,h}_{\mathbf{m}} \in V^{b,h}_{\mathbf{m}}(\mathcal{T}_\Omega, \{\mathcal{T}^i_h\})$ and $u^{b,h}_{\mathbf{m}^+}, z^{b,h}_{\mathbf{m}^+} \in V^{b,h}_{\mathbf{m}^+}(\mathcal{T}_\Omega, \{\mathcal{T}^i_h\})$, where $V^{b,h}_{\mathbf{m}}(\mathcal{T}_\Omega, \{\mathcal{T}^i_h\})$ and $V^{b,h}_{\mathbf{m}^+}(\mathcal{T}_\Omega, \{\mathcal{T}^i_h\})$ are defined according to (5). Then, it suffices to evaluate the quantity $(\delta z^{b,h}_{\mathbf{m}\mathbf{m}^+})^T K \delta u^{b,h}_{\mathbf{m}\mathbf{m}^+}$, with $\delta z^{b,h}_{\mathbf{m}\mathbf{m}^+} = z^{b,h}_{\mathbf{m}^+} - z^{b,h}_{\mathbf{m}}$, $\delta u^{b,h}_{\mathbf{m}\mathbf{m}^+} = u^{b,h}_{\mathbf{m}^+} - u^{b,h}_{\mathbf{m}}$, and where $K$ is the stiffness matrix associated with the enriched formulation (9). Notice that the matrix $K$ is already available and does not need additional computations.

We address below the two distinct steps of the **m**-adaptive procedure we are proposing.

#### 3.2.1 Phase 1: subdomain identification

The subdomains $\Omega_i$ are selected once and for all at the beginning of the **m**-adaptive procedure via a *thresholding* technique.

For this purpose, we begin with the uniform framework, as advocated in [16, 31]: we compute the value of $\eta^b_{\mathbf{m}\mathbf{m}^+}$ by employing $\widetilde{m}$ and $\widetilde{m}^+$ modes on the whole $\Omega$[2]. To contain the computational costs, it is worth choosing small values for both $\widetilde{m}$ and $\widetilde{m}^+$. In particular, we compute the estimator normalized by its maximum value, that we denote by $\breve{\eta}^b_{\widetilde{m}\widetilde{m}^+}$. In this way, we may assume the estimate to be in the range $[\breve{\eta}^b_{\widetilde{m}\widetilde{m}^+,\min}, 1]$, with $\breve{\eta}^b_{\widetilde{m}\widetilde{m}^+,\min}$ the minimum value assumed by the normalized estimator on $\Omega$.

We select a threshold $\phi \in (0,1)$. If the threshold is less than $\breve{\eta}^b_{\widetilde{m}\widetilde{m}^+,\min}$, this means that the initial guess for the modal truncation is too coarse; we refine uniformly $\widetilde{m}$ and $\widetilde{m}^+$ and recompute the normalized estimator. Hereafter, we assume $\phi \geq \breve{\eta}^b_{\widetilde{m}\widetilde{m}^+,\min}$.

[2]We usually set $\widetilde{m}^+ = m + 2$; due to the parity of sinusoidal functions the simplest choice $\widetilde{m}^+ = m + 1$ is completely useless when dealing with solutions symmetric with respect to fiber $\Omega_{1D}$.

We introduce now a uniform finite element partition $\{K_l\}$ on $\Omega_{1D}$ and we assign the value $\breve{\eta}^b_{\widetilde{m}\widetilde{m}^+}\big|_{K_l}$ to the barycenter of $K_l$. We denote by $\xi_j$, with $j \in \{1,\dots,\hat{s}\}$, the intersections between $\breve{\eta}^b_{\widetilde{m}\widetilde{m}^+}$ and $\phi$, and by $\sigma_j$ the corresponding closest finite element node. The set $\{\sigma_j\}$ induces the partition $\mathcal{T}_\Omega = \{\Omega_i\}_{i=1}^s$, with $s \equiv \hat{s}+1$, $\sigma_0 = x_0$, $\sigma_s = x_1$, and with $\Sigma_j = \{\sigma_j\} \times \gamma_{\sigma_j}$ the interface between $\Omega_j$ and $\Omega_{j+1}$.

**Remark 3.2** *There are two critical situations that may occur when selecting the threshold $\phi$. If a root of the equation $\phi - \breve{\eta}^b_{\widetilde{m}\widetilde{m}^+} = 0$ has multiplicity strictly greater than one, the algorithm for identifying the subdomains fails. This can be avoided by a proper selection of $\phi$ driven by a check of the first derivative of $\breve{\eta}^b_{\widetilde{m}\widetilde{m}^+}$. On the other hand, if $\breve{\eta}^b_{\widetilde{m}\widetilde{m}^+}$ presents several oscillations around a range of values, these values are not good candidates to be the threshold, since this would lead to the identification of many subdomains, making the numerical procedure ineffective. As a limit case, if the oscillation ranges over the entire codomain, the present approach is not appropriate. In the numerical simulations illustrated later on, the threshold has been selected by direct inspection to avoid all these critical situations.*

At the end of this thresholding approach, we can also provide the initial guess $\mathbf{m}^{(0)} = \{m_i^{(0)}\}_{i=1}^s \in [\mathbb{N}^+]^s$ for the modal multi-index which feeds the second phase of the **m**-adaptive procedure. In particular,

$$m_i^{(0)} = \begin{cases} \widetilde{m} & \text{if} \quad \breve{\eta}^b_{\widetilde{m}\widetilde{m}^+}\big|_{K_l} < \phi, \ \forall K_l \text{ s.t. } K_l \cap \Omega_{1D,i} \neq \emptyset, \\ \widetilde{m}+\delta & \text{if} \quad \breve{\eta}^b_{\widetilde{m}\widetilde{m}^+}\big|_{K_l} \geq \phi, \ \forall K_l \text{ s.t. } K_l \cap \Omega_{1D,i} \neq \emptyset, \end{cases}$$

with $\delta \in \mathbb{N}^+$ the modal update. Likewise, we define the initial guess $\mathbf{m}^{+\,(0)}$ for the multi-index $\mathbf{m}^+$.

### 3.2.2 Phase 2: mode adaptivity

Once we have detected the subdomains, we compute the modal multi-index $\mathbf{m}$ to satisfy the requirement $\eta^b_{\mathbf{m}\mathbf{m}^+} \leq$ `TOLM`. Starting from the initial guess obtained at the end of phase 1, we update $\mathbf{m}$ relying upon an equidistribution criterion on the subdomains $\Omega_i$. This means that we demand a uniform error distribution over $\mathcal{T}_\Omega$, i.e., $\eta^{b,i}_{\mathbf{m}\mathbf{m}^+} =$ `TOLM`$/s$, where $\eta^{b,i}_{\mathbf{m}\mathbf{m}^+} = \eta^b_{\mathbf{m}\mathbf{m}^+}\big|_{\Omega_i}$ denotes the modeling error estimator associated with the subdomain $\Omega_i$ for $i \in \{1,\dots,s\}$ (see lines `9.` and `11.` in the subsequent pseudo-code).
The main steps of the mode adaptivity procedure are listed below:

`1.` `set` $\mathbf{m} = \mathbf{m}^{(0)}$ `and` $\mathbf{m}^+ = \mathbf{m}^{+\,(0)}$`;`

`2.` `solve the primal problems` (4) `and` (9)`;`

`3.` `solve the dual problems` (8) `and` (10)`;`

`4.` `compute` $\eta^b_{\mathbf{m}\mathbf{m}^+}$ `via` (14)`;`

5. if $\eta^b_{\mathbf{mm}^+} \leq$ TOLM, break;
6. for k=1:NmaxM
    7. for i=1:s
        8. compute $\eta^{b,\mathtt{i}}_{\mathbf{mm}^+}$;
        9. if $\eta^{b,\mathtt{i}}_{\mathbf{mm}^+} >$ deltaM1$\dfrac{\mathtt{TOLM}}{\mathtt{s}}$
            10. $m_{\mathtt{i}}^{(\mathtt{k})} = m_{\mathtt{i}}^{(\mathtt{k}-1)} + \delta$; $m_{\mathtt{i}}^{+\,(\mathtt{k})} = m_{\mathtt{i}}^{+\,(\mathtt{k}-1)} + \delta$;
        11. elseif $\eta^{b,\mathtt{i}}_{\mathbf{mm}^+} \leq$ deltaM2$\dfrac{\mathtt{TOLM}}{\mathtt{s}}$
            12. $m_{\mathtt{i}}^{(\mathtt{k})} = \max(1, m_{\mathtt{i}}^{(\mathtt{k}-1)} - \delta)$, $m_{\mathtt{i}}^{+,(\mathtt{k})} = \max(1, m_{\mathtt{i}}^{+,(\mathtt{k}-1)} - \delta)$;
            end
    13. solve the primal problems (4) and (9);
    14. solve the dual problems (8) and (10);
    15. compute $\eta^b_{\mathbf{mm}^+}$ via (14);
    16. if $\eta^b_{\mathbf{mm}^+} \leq$ TOLM, break;
    end

As usual, we have introduced a maximum number NmaxM of allowed iterations. If this procedure terminates within this number, the piecewise hierarchically reduced solution $u^b_{\mathbf{m}}$ associated with the detected multi-index partition is such that $J(u^b_{\mathbf{m}}) \simeq J(u)$ within a tolerance equal to TOLM.

We may notice that our algorithm takes care of both model refinement and coarsening. When coarsening, we force the minimal value of admissible modes to be at least equal to one (line 12. of the pseudo-code).
In particular, the parameters deltaM1 and deltaM2 limit the occurrence of model refinement and coarsening, respectively for the sake of algorithm robustness (and computational efficiency).

The control of the fulfillment of the desired tolerance for the estimator is performed at steps 5. and 16.: in the first case, we check if the initial guess $\mathbf{m}^{(0)}$ predicts a sufficiently rich model; in 16. we make the same check after the new prediction for $\mathbf{m}$ at steps 10. and 12..

### 3.3 Numerical assessment of the m-adaptive procedure

We present in this section a test case where the analytical solution is known so to check the robustness of the estimator $\eta^b_{\mathbf{mm}^+}$ as well as of the $\mathbf{m}$-adaptive procedure both from a qualitative and a quantitative viewpoint. The numerical validation here and in the entire paper is carried out in 2D. In particular, we employ affine finite elements to discretize the problem along $\Omega_{1D}$, while we resort to sinusoidal functions to model the transverse dynamics. The increment $\delta$ is set to 1. We finally evaluate the integrals of the sine functions via suitable Gaussian quadrature formulas, based on, at least, four quadrature nodes per wavelenght.

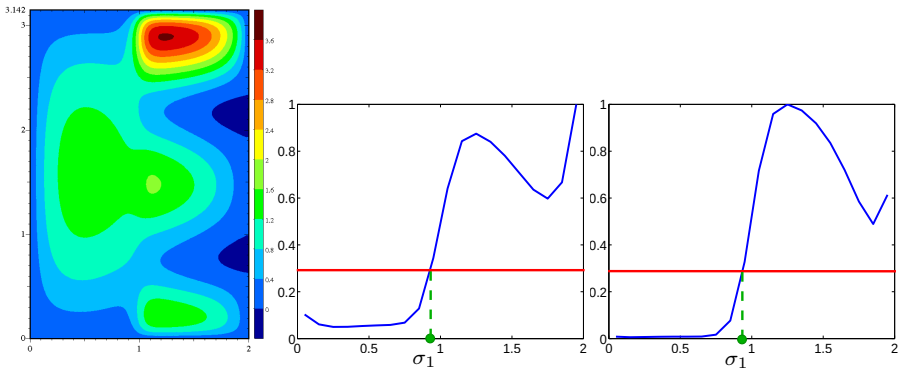


Figure 3: Full solution (left); normalized estimator $\breve{\eta}^b_{13}$ (center) and $\breve{\eta}^b_{35}$ (right)

We solve the standard Poisson problem $-\Delta u = f$ on the rectangular domain $\Omega = (0,2) \times (0,\pi)$, completed with full homogeneous Dirichlet boundary conditions. In particular, the source term $f$ is chosen such that the exact solution $u \in V \equiv H^1_0(\Omega)$ to the full problem (1) is

$$u(x,y) = \frac{(256 - x^8)(256 - (2-x)^8)}{64800} \left\{ \frac{100}{247} y(\pi - y)(2 - x) \right.$$
$$\left. + y\Big(\frac{\pi}{5} - y\Big)\Big(\frac{\pi}{3} - y\Big)\Big(\frac{3}{5}\pi - y\Big)\Big(\frac{3}{4}\pi - y\Big)(\pi - y)\big(1 + \tanh(10x - 10)\big) \right\}.$$

This particular solution has been selected to trigger different transverse dynamics in different parts of the computational domain. Figure 3, left shows the contour plots of $u$ approximated via a 2D finite element scheme on a uniform unstructured grid of about 25300 elements. On the left hand side of the domain, the solution exhibits a transverse behavior characterized by low frequencies, as opposed to the right hand side, where higher frequencies are active. In this example, we control the mean value of the full solution on $\Omega$, i.e., we choose the goal functional in (8) as $J_{mean}(v) = [\mathrm{meas}(\Omega)]^{-1} \int_\Omega v(x,y)\, d\mathbf{z}$, for any $v \in L^1(\Omega)$. Due to the self-adjointness of the Poisson equation, the dual problem coincides with the primal one except for the forcing term which is the density function $j(x,y) = [\mathrm{meas}(\Omega)]^{-1}\chi_\Omega(x,y)$ associated with $J_{mean}$. Full homogeneous Dirichlet boundary conditions complete the dual formulation.

Let us introduce some preliminary heuristic considerations about the saturation assumption (12).

*Calibration of the saturation constant.* In this particular case, we can take advantage of the explicit analytic solution to provide an estimate for $\beta_{\mathbf{m}}$ in (12). More precisely, we compute the errors $e^b_{\mathbf{m}}$ and $e^b_{\mathbf{m}^+}$ and estimate the constant $\beta_{\mathbf{m}}$ via the quotient $|J(e^b_{\mathbf{m}^+})|/|J(e^b_{\mathbf{m}})|$. We do this in the uniform framework, to avoid the estimate to be affected by the possible non-conformity of the reduced model so that the actual estimator for $\beta_{\mathbf{m}}$ in (12) becomes

$\beta_m^{\text{estim}} = |J(e^b_{m^+})|/|J(e^b_m)|$, with $e^b_m$ and $e^b_{m^+}$ the modeling errors associated with a uniform Hi-Mod reduction.

Table 1 displays the values of $\beta_m^{\text{estim}}$ for different choices of the uniform modal indices and for different (uniform) finite element discretizations of the supporting domain $\Omega_{1D}$. As expected, the value of $\beta_m^{\text{estim}}$ gets progressively closer to one when $m$ and $m^+$ increase. Notice that the choice of the discretization step $h$ has only a moderate effect on the estimated value. In particular, we pessimistically select 0.8971 as approximate value for $\beta_{\mathbf{m}}$ in (12). Noticing that $1/(1-\beta_{\mathbf{m}}) = 9.7181$, in the numerical test presented hereafter the goal error $|J(e^b_{\mathbf{m}})|$ is estimated by $9.7181\,\eta^b_{\mathbf{mm}^+}$. Should we get rid of the factor $1/(1-\beta_{\mathbf{m}})$ in (13), the actual error would be underestimated.[3]

Table 1: Approximate values $\beta_m^{\text{estim}}$ for the saturation constant in (12)

| $m$ | $m^+$ | $h = 0.1$ | $h = 0.05$ | $h = 0.025$ |
|---|---|---|---|---|
| 1 | 3 | 0.7031 | 0.7001 | 0.6994 |
| 3 | 5 | 0.6141 | 0.6088 | 0.6074 |
| 5 | 7 | 0.7941 | 0.7895 | 0.7883 |
| 7 | 9 | 0.8971 | 0.8942 | 0.8935 |

*The* **m***-adaptive procedure.* For the input parameters we select $\widetilde{m} = 1$, $\widetilde{m}^+ = 3$; $\phi = 0.3$; $\delta = 1$; `TOLM` $= 0.14$; `deltaM1` $= 0.5$; `deltaM2` $= 1.5$; `NmaxM` $= 10$; a uniform finite element partition of size $h = 0.1$ is introduced on $\Omega_{1D}$.

The first phase of the procedure identifies the point $\sigma_1 = 0.9$ (see Figure 3, center), namely the two subdomains $\Omega_1 = (0, 0.9) \times (0, \pi)$ and $\Omega_2 = (0.9, 2) \times (0, \pi)$. Moreover, the modal multi-indices predicted as initial guess for the mode adaptivity are the pairs $\mathbf{m}^{(0)} = \{1, 2\}$ and $\mathbf{m}^{+\,(0)} = \{3, 4\}$, respectively.

The second phase of the **m**-adaptive procedure converges after five iterations, with the final prediction for $\mathbf{m} = \mathbf{m}^{(5)} = \{1, 7\}$; in particular, a single mode is employed on $\Omega_1$ for the whole adaptive procedure, while the number of modal functions gradually increases from 2 to 7 in $\Omega_2$. The final mode distribution reasonably matches the solution heterogeneity. Four domain decomposition iterations are on average demanded to reach a tolerance of $10^{-3}$ at the interface $\Sigma_1 = \{0.9\} \times \gamma_{0.9}$.

Figure 4 collects the piecewise hierarchically reduced solution together with the distribution of the corresponding error estimator for the starting guess and for the odd iterations of the adaptive procedure. As expected, a model discontinuity occurs at the interface $\Sigma_1$ since $m_1 < m_2$. Concerning the error estimator distribution, the blue line corresponds to $\eta^{b,1}_{\mathbf{mm}^+}$ while the green one is associated with $\eta^{b,2}_{\mathbf{mm}^+}$.

Table 2 provides some more quantitative information. The sequence of columns

[3] In practice, when the exact solution is not known, one can simply set $\beta_{\mathbf{m}}$ to zero or introduce an appropriate "safety factor" in the error estimation.

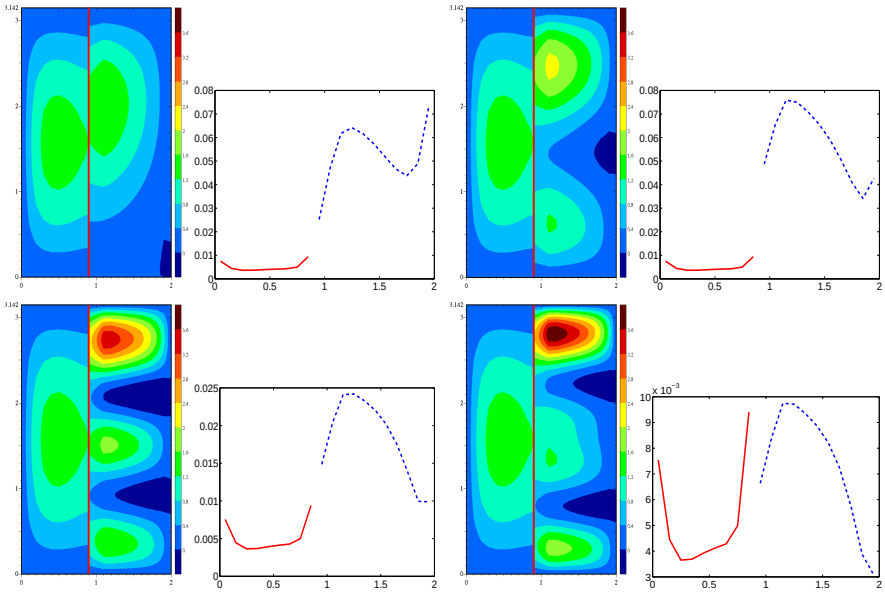

Figure 4: Piecewise hierarchically reduced solution and distribution of the corresponding modeling error estimator for $\mathbf{m} = \{1, 2\}$, $\mathbf{m}^+ = \{3, 4\}$ (top-left), $\mathbf{m} = \{1, 3\}$, $\mathbf{m}^+ = \{3, 5\}$ (top-right), $\mathbf{m} = \{1, 5\}$, $\mathbf{m}^+ = \{3, 7\}$ (bottom-left), $\mathbf{m} = \{1, 7\}$, $\mathbf{m}^+ = \{3, 9\}$ (bottom-right)

gathers the iteration number `k`, the modal multi-index $\mathbf{m} = \{m_1, m_2\}$, the exact goal error and the value of the estimator $1/(1 - \beta_{\mathbf{m}})\, \eta^b_{\mathbf{mm}^+}$, with $\beta_{\mathbf{m}} = 0.8971$. We omit to report on the even iterations, since they do not bring substantial benefit when $m_2$ commutes from an odd to an even value. This is justified by the choice of the goal functional. As a matter of fact, the parity of sinusoidal functions $\sin(qy)$, with $q$ even, implies that they do not contribute to control the mean value of the solution.
The error estimator slightly over-estimates the actual error as confirmed by the values of the modeling effectivity index $\text{E.I.}_{\mathbf{m}} = \eta^b_{\mathbf{mm}^+}/[(1 - \beta_{\mathbf{m}})\, |J(u - u^b_{\mathbf{m}})|]$ displayed in Table 3, for different choices of the finite element discretization step $h$. The effectivity index gradually diminishes while the mode adaptivity proceeds. A finer finite element discretization does not improve the quality of the modeling error estimator in this case. This most likely points out that the discretization error is dominated by the modal discretization, so that the reduction of the mesh size $h$ is not useful and only deteriorates the conditioning of the problem.

In order to test the sensitivity of the **m**-adaptive procedure to the initial guess for the uniform modal indices $\widetilde{m}$ and $\widetilde{m}^+$, we present also the results associated with the choices $\widetilde{m} = 3$, $\widetilde{m}^+ = 5$ and $\widetilde{m} = 5$, $\widetilde{m}^+ = 7$, while preserving the same values for all the other input parameters. For both the pairs of indices, the same

Table 2: Quantitative information about the second phase of the **m**-adaptive procedure for $\widetilde{m} = 1$, $\widetilde{m}^+ = 3$

| k | $\mathbf{m}$ | $\lvert J(u - u^b_{\mathbf{m}})\rvert$ | $\eta^b_{\mathbf{m}\mathbf{m}^+}$ |
|---|---|---|---|
| 1 | $\{1,3\}$ | $1.42 \cdot 10^{-1}$ | $6.75 \cdot 10^{-1}$ |
| 3 | $\{1,5\}$ | $7.81 \cdot 10^{-2}$ | $2.46 \cdot 10^{-1}$ |
| 5 | $\{1,7\}$ | $5.80 \cdot 10^{-2}$ | $1.27 \cdot 10^{-1}$ |

Table 3: $\text{E.I.}_{\mathbf{m}}$ for different discretization steps $h$

| k | $h = 0.1$ | $h = 0.05$ | $h = 0.025$ |
|---|---|---|---|
| 1 | 4.75 | 5.71 | 6.13 |
| 3 | 3.15 | 4.45 | 5.17 |
| 5 | 2.18 | 3.60 | 4.58 |

subdomains as in Figure 4 are identified ($\Omega_1 = (0, 0.9)\times(0, \pi)$ and $\Omega_2 = (0.9, 2)\times(0, \pi)$), with an initial guess for the mode adaptivity given consequently by $\mathbf{m}^{(0)} = \{3, 4\}$, $\mathbf{m}^{+\,(0)} = \{5, 6\}$ and $\mathbf{m}^{(0)} = \{5, 6\}$, $\mathbf{m}^{+\,(0)} = \{7, 8\}$, respectively.

The number of **m**-adaptive iterations reduces in both the cases. For $\widetilde{m} = 3$, $\widetilde{m}^+ = 5$, the tolerance $\texttt{TOLM} = 0.14$ is achieved after three iterations with the final prediction $\mathbf{m} = \mathbf{m}^{(3)} = \{2, 7\}$ (see Figure 5, left): at the first iteration the number of modes on $\Omega_1$ decreases by one and it remains unchanged in the successive iterations; on the contrary, the number of modal functions on $\Omega_2$ increases from 4 to 7.
For $\widetilde{m} = 5$, $\widetilde{m}^+ = 7$, a single iteration yields a reduced model with an error estimator $\eta^b_{\mathbf{m}\mathbf{m}^+}$ below tolerance, with a final prediction for the modal multi-index equal to $\mathbf{m} = \mathbf{m}^{(1)} = \{4, 7\}$ (see Figure 5, right).
The convergence of the domain decomposition algorithm with an accuracy of $10^{-3}$ is guaranteed also in these two last cases after an average of four iterations.

Tables 4 and 5 collect the most significant results concerning these two cases. We stress the improvement in the values of $\text{E.I.}_{\mathbf{m}}$: in particular, the choice $\widetilde{m} = 5$, $\widetilde{m}^+ = 7$ leads to an actual robust modeling error estimator.

Table 4: Quantitative information about the second phase of the **m**-adaptive procedure for $\widetilde{m} = 3$, $\widetilde{m}^+ = 5$

| k | $\mathbf{m}$ | $\lvert J(u - u^b_{\mathbf{m}})\rvert$ | $\eta^b_{\mathbf{m}\mathbf{m}^+}$ | $\text{E.I.}_{\mathbf{m}}$ |
|---|---|---|---|---|
| 0 | $\{3,4\}$ | $1.53 \cdot 10^{-1}$ | $5.73 \cdot 10^{-1}$ | 3.74 |
| 1 | $\{2,5\}$ | $7.81 \cdot 10^{-2}$ | $2.46 \cdot 10^{-1}$ | 3.15 |
| 3 | $\{2,7\}$ | $5.80 \cdot 10^{-2}$ | $1.27 \cdot 10^{-1}$ | 2.19 |

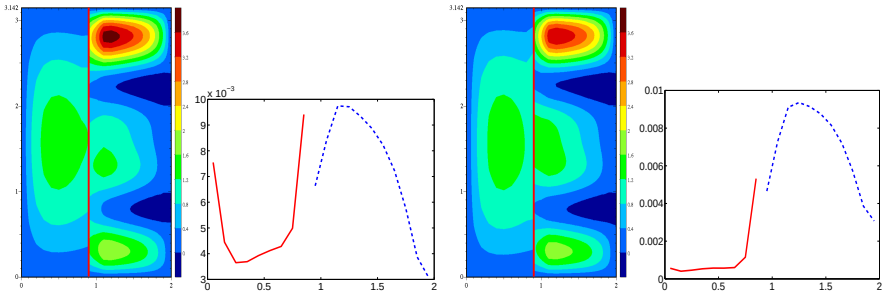

Figure 5: Piecewise hierarchically reduced solution and distribution of the corresponding modeling error estimator for $\mathbf{m} = \{2, 7\}$, $\mathbf{m}^+ = \{4, 9\}$ (left) and for $\mathbf{m} = \{4, 7\}$, $\mathbf{m}^+ = \{6, 9\}$ (right)

Table 5: Quantitative information about the second phase of the **m**-adaptive procedure for $\widetilde{m} = 5$, $\widetilde{m}^+ = 7$

| k | $\mathbf{m}$ | $\lvert J(u - u^b_{\mathbf{m}})\rvert$ | $\eta^b_{\mathbf{m}\mathbf{m}^+}$ | E.I.$_{\mathbf{m}}$ |
|---|---|---|---|---|
| 0 | $\{5, 6\}$ | $9.45 \cdot 10^{-2}$ | $1.88 \cdot 10^{-1}$ | 1.99 |
| 1 | $\{4, 7\}$ | $6.92 \cdot 10^{-2}$ | $8.65 \cdot 10^{-2}$ | 1.25 |

# 4 Automatic piecewise Hi-Mod reduction coupled with mesh adaptivity

We remove now any assumption on the size of the mesh for the finite element discretization of the mainstream dynamics.
For this purpose, we introduce the *global error* $e^{b,h}_{\mathbf{m}} = u - u^{b,h}_{\mathbf{m}} \in H^1(\Omega, \mathcal{T}_\Omega)$, which collects the contribution of both the modeling error ($e^b_{\mathbf{m}} = u - u^b_{\mathbf{m}}$) and the discretization error ($\varepsilon^{b,h}_{\mathbf{m}} = u^b_{\mathbf{m}} - u^{b,h}_{\mathbf{m}}$). An *a priori* analysis for the global error is furnished in [31, Section 4.2.2], under the assumption that the Dirichlet-Neumann scheme converges.

## 4.1 A goal-oriented global error estimator

We adapt both the hierarchically reduced model and the discretization along $\Omega_{1D}$ to provide a reliable approximation, $J(u^{b,h}_{\mathbf{m}})$, of the exact goal value $J(u)$, so that the estimated error $|J(u) - J(u^{b,h}_{\mathbf{m}})|$ is below a global tolerance `TOL`. To this aim, it is crucial to derive an *a posteriori* estimator for the global error where the contributions of the modeling and of the discretization errors are kept separated.

We can prove this first result:

**Proposition 4.1** *Under saturation assumption* (12)*, the following inequality*

*holds*

$$|J(e^{b,h}_{\mathbf{m}})| \leq \frac{1+\beta_{\mathbf{m}}}{1-\beta_{\mathbf{m}}} \left( |J(\delta u^{b}_{\mathbf{m}\mathbf{m}^+})| + |J(\varepsilon^{b,h}_{\mathbf{m}})| \right) \tag{15}$$

*for any* $\mathbf{m}$ *and* $\mathbf{m}^+ \in [\mathbb{N}^+]^s$ *with* $\mathbf{m}^+ > \mathbf{m} \geq \mathbf{M}_0$, $\mathbf{M}_0$ *being the modal multi-index involved in Proposition 3.2.*

**Proof.** We split $e^{b,h}_{\mathbf{m}}$ as follows

$$e^{b,h}_{\mathbf{m}} = e^{b}_{\mathbf{m}} + \varepsilon^{b,h}_{\mathbf{m}} = e^{b}_{\mathbf{m}^+} + \delta u^{b}_{\mathbf{m}\mathbf{m}^+} + \varepsilon^{b,h}_{\mathbf{m}}, \tag{16}$$

with $e^{b}_{\mathbf{m}^+} = u - u^{b}_{\mathbf{m}^+}$. We distinguish two cases.

*case a)* $|J(e^{b}_{\mathbf{m}})| \geq |J(\varepsilon^{b,h}_{\mathbf{m}})|$: by exploting (16), assumption (12) and the linearity of $J$, we get

$$\begin{aligned} |J(e^{b}_{\mathbf{m}})| - |J(\varepsilon^{b,h}_{\mathbf{m}})| &\leq |J(e^{b}_{\mathbf{m}} + \varepsilon^{b,h}_{\mathbf{m}})| = |J(e^{b}_{\mathbf{m}^+} + \delta u^{b}_{\mathbf{m}\mathbf{m}^+} + \varepsilon^{b,h}_{\mathbf{m}})| \\ &\leq \beta_{\mathbf{m}} |J(e^{b}_{\mathbf{m}})| + |J(\delta u^{b}_{\mathbf{m}\mathbf{m}^+})| + |J(\varepsilon^{b,h}_{\mathbf{m}})|, \end{aligned} \tag{17}$$

yieding

$$|J(e^{b}_{\mathbf{m}})| \leq \frac{1}{1-\beta_{\mathbf{m}}} \left\{ |J(\delta u^{b}_{\mathbf{m}\mathbf{m}^+})| + 2|J(\varepsilon^{b,h}_{\mathbf{m}})| \right\}. \tag{18}$$

Now, by suitably combining (17) with (18), we obtain

$$|J(e^{b,h}_{\mathbf{m}})| \leq \frac{1}{1-\beta_{\mathbf{m}}} |J(\delta u^{b}_{\mathbf{m}\mathbf{m}^+})| + \frac{1+\beta_{\mathbf{m}}}{1-\beta_{\mathbf{m}}} |J(\varepsilon^{b,h}_{\mathbf{m}})|, \tag{19}$$

that is (15), since $\beta_{\mathbf{m}}$ is a positive constant.

*case b)* $|J(e^{b}_{\mathbf{m}})| < |J(\varepsilon^{b,h}_{\mathbf{m}})|$: we move from the second splitting in (16); the saturation assumption together with inequalities $|J(e^{b}_{\mathbf{m}})| < |J(\varepsilon^{b,h}_{\mathbf{m}})|$ and $\beta_{\mathbf{m}} < 1$, yields

$$\begin{aligned} |J(e^{b,h}_{\mathbf{m}})| &\leq \beta_{\mathbf{m}} |J(e^{b}_{\mathbf{m}})| + |J(\delta u^{b}_{\mathbf{m}\mathbf{m}^+})| + |J(\varepsilon^{b,h}_{\mathbf{m}})| \\ &\leq \frac{1+\beta_{\mathbf{m}}}{1-\beta_{\mathbf{m}}} |J(\varepsilon^{b,h}_{\mathbf{m}})| + \frac{1}{1-\beta_{\mathbf{m}}} |J(\delta u^{b}_{\mathbf{m}\mathbf{m}^+})|, \end{aligned}$$

so that we recover relation (19), i.e. (15), also in this case. □ Moving from (15), we may choose as *a posteriori* estimator for the global functional error $|J(e^{b,h}_{\mathbf{m}})|$ the quantity

$$|J(\delta u^{b}_{\mathbf{m}\mathbf{m}^+})| + |J(\varepsilon^{b,h}_{\mathbf{m}})|. \tag{20}$$

In particular, relation (15) provides us with the corresponding reliability estimate. As expected, the modeling and the discretization contributions in (20) are distinct. In particular, the former component coincides with (14).

To prove the efficiency of (20) we have to add a further hypothesis, which essentially relates the modeling with the discretization error.

**Proposition 4.2** *Let us assume that there exists a positive constant* $\gamma < 1$ *such that*

$$|J(\varepsilon^{b,h}_{\mathbf{m}})| \leq \gamma |J(e^{b}_{\mathbf{m}})|. \tag{21}$$

*Then, under saturation assumption* (12)*, it holds*

$$|J(e^{b,h}_{\mathbf{m}})| \geq \frac{1-\gamma}{3+\beta_{\mathbf{m}}-\gamma}\left[|J(\delta u^{b}_{\mathbf{m}\mathbf{m}^+})| + |J(\varepsilon^{b,h}_{\mathbf{m}})|\right] \tag{22}$$

*for any* $\mathbf{m}$ *and* $\mathbf{m}^+ \in [\mathbb{N}^+]^s$ *with* $\mathbf{m}^+ > \mathbf{m} \geq \mathbf{M}_0$*, and with* $\mathbf{M}_0$ *the modal multi-index involved in* (12)*.*

**Proof.** We bound both $|J(\delta u^{b}_{\mathbf{m}\mathbf{m}^+})|$ and $|J(\varepsilon^{b,h}_{\mathbf{m}})|$ in terms of the global error $|J(e^{b,h}_{\mathbf{m}})|$. From (21) and (16), it immediately follows

$$\big(1-\gamma\big)\,|J(e^{b}_{\mathbf{m}})| \leq |J(e^{b,h}_{\mathbf{m}})|. \tag{23}$$

By combining this relation with the saturation assumption and with the definition $\delta u^{b}_{\mathbf{m}\mathbf{m}^+} = e^{b}_{\mathbf{m}} - e^{b}_{\mathbf{m}^+}$, we get

$$|J(\delta u^{b}_{\mathbf{m}\mathbf{m}^+})| \leq |J(e^{b}_{\mathbf{m}})| + |J(e^{b}_{\mathbf{m}^+})| \leq (1+\beta_{\mathbf{m}})\,|J(e^{b}_{\mathbf{m}})| \leq \frac{1+\beta_{\mathbf{m}}}{1-\gamma}\,|J(e^{b,h}_{\mathbf{m}})|. \tag{24}$$

As for the term $|J(\varepsilon^{b,h}_{\mathbf{m}})|$, since $\varepsilon^{b,h}_{\mathbf{m}} = e^{b,h}_{\mathbf{m}} - e^{b}_{\mathbf{m}}$ and thanks again to relation (23), we have

$$|J(\varepsilon^{b,h}_{\mathbf{m}})| \leq |J(e^{b,h}_{\mathbf{m}})| + |J(e^{b}_{\mathbf{m}})| \leq \frac{2-\gamma}{1-\gamma}\,|J(e^{b,h}_{\mathbf{m}})|. \tag{25}$$

By adding (24) and (25), we obtain (22). □

Notice that the efficiency constant in (22) is always strictly greater than $(1-\gamma)/(4-\gamma) > 0$.

**Remark 4.1** *Assumption* (21) *essentially establishes a ratio between the modeling and the discretization errors. It can be interpreted as a* sufficient grid resolution *requirement. Moreover, even though* $\gamma$ *may depend on* $h$ *and* $\mathbf{m}$*, we do not add any index to* $\gamma$ *for easiness of notation. As shown in Section 4.2, relation* (21) *will be advantageously exploited in setting up the model-mesh adaptive procedure.*

While the model contribution in (20) coincides exactly with the modeling error estimator in (14), we have to properly estimate the discretization contribution $|J(\varepsilon^{b,h}_{\mathbf{m}})|$. The goal-oriented analysis advocated, e.g., in [4, 7, 18, 20, 28] cannot be applied straightforwardly to the Hi-Mod reduction context. The possible presence of non-conformity as well as the intrinsic dimensionally hybrid nature of the reduced model calls for some specific adjustements.

For the sake of simplicity, we now assume $\Omega \subset \mathbb{R}^2$ and we complete problem (1) with full homogeneous Dirichlet boundary conditions.
We denote by $R^i_l$ the region of $\Omega_i$ defined by $\bigcup_{x\in K^i_l}\{x\}\times\gamma_x$ with $\{K^i_l\}_{l=1}^{n_i}$ defined as in Section 2.2, while the interface between $R^i_t$ and $R^i_{t+1}$ is indicated by $\zeta^i_t$, for $t \in \{1,\dots,n_i-1\}$ and $i \in \{1,\dots,s\}$ (see Figure 6).

Then, we define the *internal* and the *boundary* residual associated with the piecewise hierarchically reduced discrete solution $u^{b,h}_{\mathbf{m}}$ and with $R^i_l$, given by

$$r_{R^i_l}(u^{b,h}_{\mathbf{m}}) = \big(f - \mathcal{A}_i u^{b,h}_{\mathbf{m}}\big)\big|_{R^i_l} \tag{26}$$

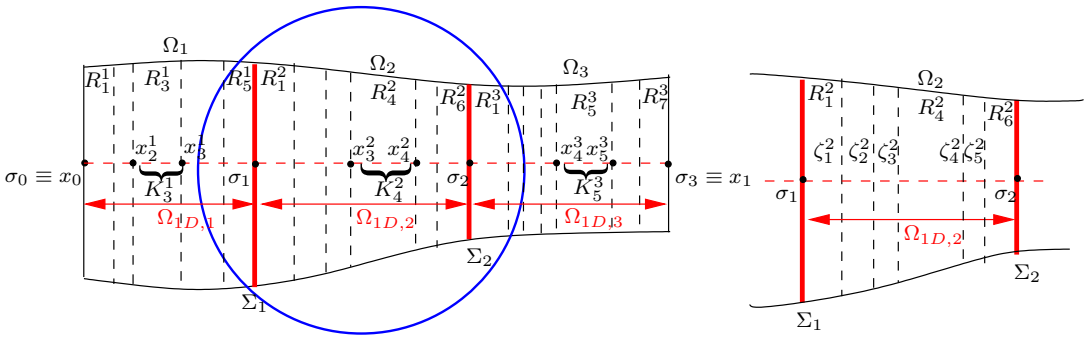


Figure 6: Partition of $\Omega \subset \mathbb{R}^2$ into $s = 3$ subdomains (left) and zoom on the highlighted subdomain (right)

and

$$j_{R_l^i} = \begin{cases} [\partial_\nu u_{\mathbf{m}}^{b,h}]_e & \text{if } e \equiv \zeta_t^i \quad \text{with} \quad t \in \{1, \dots, n_i - 1\} \\ 0 & \text{if } e \cap \Gamma_* \neq \emptyset \\ 0 & \text{if } e \equiv \Sigma_{i-1}, \Sigma_i, \end{cases} \tag{27}$$

respectively, with $l \in \{1, \dots, n_i\}$ and $i \in \{1, \dots, s\}$, where $\mathcal{A}_i$ represents the differential operator inducing the bilinear form $a_i(\cdot, \cdot)$, $[\partial_\nu u_{\mathbf{m}}^{b,h}]_e$ is the jump of the (co)-normal derivative of $u_{\mathbf{m}}^{b,h}$ across $e \subset \partial R_l^i$, and where $\Sigma_0 \equiv \Gamma_0$, $\Sigma_s = \Gamma_1$. We denote by $\{\partial_\nu u_{\mathbf{m}}^{b,h}\}_e$ the mean of $\partial_\nu u_{\mathbf{m}}^{b,h}$ across the generic edge portion $e$ and by

$$\widetilde{K}_l^i = \begin{cases} K_1^i \cup K_2^i, & \text{for } l = 1, \\ K_{l-1}^i \cup K_l^i \cup K_{l+1}^i & \text{for } l \in \{2, \dots, n_i - 1\}, \\ K_{n_i-1}^i \cup K_{n_i}^i & \text{for } l = n_i \end{cases} \tag{28}$$

the patch associated with the subinterval $K_l^i$, for $l \in \{1, \dots, n_i\}$ and $i \in \{1, \dots, s\}$. Finally, let $\mathcal{P}_{\Sigma_j}$ be the $L^2$-projection operator onto the interface space $\Xi_{m_\perp^j} = span\{\varphi_k(\psi_{\sigma_j}(y))\}_{k=1}^{m_\perp^j}$, with $m_\perp^j = \min(m_j, m_{j+1})$ and $j \in \{1, \dots, s-1\}$.

We have now all the ingredients to prove the following result.

**Proposition 4.3** *The following inequality holds*

$$|J(\varepsilon_{\mathbf{m}}^{b,h})| \leq C\big(\eta_h + \eta_{NCF} + \eta_{NC}\big) \tag{29}$$

*with* $C = C(\max_i m_i)$,

$$\eta_h = \sum_{i=1}^{s} \eta_{h,i} \quad \textit{with} \quad \eta_{h,i} = \sum_{l=1}^{n_i} \rho_{R_l^i}(u_{\mathbf{m}}^{b,h})\, \omega_{R_l^i}(z_{\mathbf{m}}^b - z_{\mathbf{m}}^{b,h}), \tag{30}$$

$$\eta_{NCF} = \sum_{j=1}^{s-1} \check{\rho}_{\Sigma_j}(u_{\mathbf{m}}^{b,h})\, \check{w}_{\Sigma_j}(z_{\mathbf{m}}^b - z_{\mathbf{m}}^{b,h}), \tag{31}$$

$$\eta_{NC} = \sum_{j=1}^{s-1} \rho_{\Sigma_j}(u_{\mathbf{m}}^{b,h})\, w_{\Sigma_j}(z_{\mathbf{m}}^{b} - z_{\mathbf{m}}^{b,h}), \tag{32}$$

*where $\eta_h$ controls essentially the discretization error, $\eta_{NCF}$ is related to the presence of non-conforming fluxes, $\eta_{NC}$ takes into account the non-conformity of the reduced model, with*

$$\rho_{R_l^i}(u_{\mathbf{m}}^{b,h}) = h_l^i \|r_{R_l^i}(u_{\mathbf{m}}^{b,h})\|_{L^2(R_l^i)} + \frac{1}{2}(h_l^i)^{1/2}\, \|j_{R_l^i}\|_{L^2(\partial R_l^i)}, \tag{33}$$

$$\omega_{R_l^i}(z_{\mathbf{m}}^{b} - z_{\mathbf{m}}^{b,h}) = \big(\max_{x\in K_l^i} L(x)\big)^{1/2} \sum_{k=1}^{m_i} \big\| z_k^i - z_k^{i,h} \big\|_{H^1(\widetilde{K}_l^i)}, \tag{34}$$

$$\check{\rho}_{\Sigma_j}(u_{\mathbf{m}}^{b,h}) = \big\| [\partial_\nu u_{\mathbf{m}}^{b,h}]_{\Sigma_j} \big\|_{L^2(\Sigma_j)}, \tag{35}$$

$$\begin{aligned} \check{w}_{\Sigma_j}(z_{\mathbf{m}}^{b} - z_{\mathbf{m}}^{b,h}) = {} & (h_{n_j}^j)^{1/2} \big(\max_{x\in K_{n_j}^j} L(x)\big)^{1/2} \sum_{k=1}^{m_j} \big\| z_k^j - z_k^{j,h} \big\|_{H^1(\widetilde{K}_{n_j}^j)} \\ & + (h_1^{j+1})^{1/2} \big(\max_{x\in K_1^{j+1}} L(x)\big)^{1/2} \sum_{k=1}^{m_{j+1}} \big\| z_k^{j+1} - z_k^{j+1,h} \big\|_{H^1(\widetilde{K}_1^{j+1})}, \end{aligned} \tag{36}$$

$$\rho_{\Sigma_j}(u_{\mathbf{m}}^{b,h}) = \big\| \{\partial_\nu u_{\mathbf{m}}^{b,h}\}_{\Sigma_j} - \mathcal{P}_{\Sigma_j}\{\partial_\nu u_{\mathbf{m}}^{b,h}\} \big\|_{L^2(\Sigma_j)}, \tag{37}$$

$$\omega_{\Sigma_j}(z_{\mathbf{m}}^{b} - z_{\mathbf{m}}^{b,h}) = \check{w}_{\Sigma_j}(z_{\mathbf{m}}^{b} - z_{\mathbf{m}}^{b,h}), \tag{38}$$

*with $r_{R_l^i}(u_{\mathbf{m}}^{b,h})$, $j_{R_l^i}$ and $\widetilde{K}_l^i$ defined as in* (26), (27) *and* (28), *respectively, $L(x) = \mathrm{meas}(\gamma_x)$ as in* (2), *$h_i^l$ the length of the generic subinterval $K_l^i$ for $l \in \{1,\dots,n_i\}$ and $i \in \{1,\dots,s\}$, $z_k^i$ and $z_k^{i,h}$ the modal coefficients associated with the solution $z_{\mathbf{m}}^{b}$ to the dual problem* (8) *and with the corresponding discretization $z_{\mathbf{m}}^{b,h}$, respectively.*

**Proof.** By properly combining the dual formulation (8), the Galerkin orthogonality (7) and the reduced formulation in (4), we first get

$$\begin{aligned} |J(\varepsilon_{\mathbf{m}}^{b,h})| &= |a_{\mathcal{T}_\Omega}(\varepsilon_{\mathbf{m}}^{b,h}, z_{\mathbf{m}}^{b} - v_{\mathbf{m}}^{b,h})| = |\mathcal{F}_{\mathcal{T}_\Omega}(z_{\mathbf{m}}^{b} - v_{\mathbf{m}}^{b,h}) - a_{\mathcal{T}_\Omega}(u_{\mathbf{m}}^{b,h}, z_{\mathbf{m}}^{b} - v_{\mathbf{m}}^{b,h})| \\ &= \Big| \sum_{i=1}^{s} \Big\{ \mathcal{F}_i((z_{\mathbf{m}}^{b} - v_{\mathbf{m}}^{b,h})\big|_{\Omega_i}) - a_i(u_{\mathbf{m}}^{b,h}\big|_{\Omega_i}, (z_{\mathbf{m}}^{b} - v_{\mathbf{m}}^{b,h})\big|_{\Omega_i}) \Big\} \Big|. \end{aligned} \tag{39}$$

Now, by suitably integrating by parts on the regions $R_l^i$ and thanks to the definitions (26) and (27), we obtain

$$\begin{aligned} |J(\varepsilon_{\mathbf{m}}^{b,h})| \le {} & \sum_{i=1}^{s} \sum_{l=1}^{n_i} \Big\{ \Big| \int_{R_l^i} r_{R_l^i}(u_{\mathbf{m}}^{b,h})\, (z_{\mathbf{m}}^{b} - v_{\mathbf{m}}^{b,h})\big|_{R_l^i}\, dR_l^i \Big| \\ + {} & \frac{1}{2} \Big| \int_{\partial R_l^i} j_{R_l^i}\, (z_{\mathbf{m}}^{b} - v_{\mathbf{m}}^{b,h})\big|_{\partial R_l^i}\, d\partial R_l^i \Big| \Big\} + \sum_{j=1}^{s-1} \Big| \int_{\Sigma_j} [\partial_\nu u_{\mathbf{m}}^{b,h} (z_{\mathbf{m}}^{b} - v_{\mathbf{m}}^{b,h})]_{\Sigma_j}\, d\Sigma_j \Big|, \end{aligned} \tag{40}$$

with $[\cdot]_{\Sigma_j}$ the jump across the interface $\Sigma_j$. No contribution is associated with $\Sigma_0$ and $\Sigma_s$ due to the choice made for the boundary conditions on $\partial\Omega$.
Let us analyze, separately, the three integrals in (40). According to the definition of the spaces $V^b_{\mathbf{m}}(\mathcal{T}_\Omega)$ and $V^{b,h}_{\mathbf{m}}(\mathcal{T}_\Omega, \{\mathcal{T}^i_h\})$, we introduce the following expansions

$$(z^b_{\mathbf{m}} - v^{b,h}_{\mathbf{m}})\big|_{R^i_l} = \sum_{k=1}^{m_i} (z^i_k - v^{i,h}_k)|_{K^i_l}(x)\, \varphi_k(\psi_x(y)),$$

$$(z^b_{\mathbf{m}} - v^{b,h}_{\mathbf{m}})\big|_{\zeta^i_t} = \sum_{k=1}^{m_i} (z^i_k - v^{i,h}_k)(x^i_t)\, \varphi_k(\psi_{x^i_t}(y)).$$

Thanks to the orthonormality of the modal basis,

$$\begin{aligned} & \|z^b_{\mathbf{m}} - v^{b,h}_{\mathbf{m}}\|^2_{L^2(R^i_l)} \\ \leq\ & \widetilde{C} \sum_{k=1}^{m_i} \int_{K^i_l} \Big[ \int_{\widehat{\gamma}_1} \varphi^2_k(\widehat{y}) \left| \mathcal{J}^{-1}(x, \psi^{-1}_x(\widehat{y}) \right| d\widehat{y} \Big] [(z^i_k - v^{i,h}_k)|_{K^i_l}(x)]^2\, dx \\ \leq\ & \widetilde{C} \sum_{k=1}^{m_i} \max_{x \in K^i_l} L(x)\, \|z^i_k - v^{i,h}_k\|^2_{L^2(K^i_l)}, \end{aligned} \tag{41}$$

with $\widetilde{C} = m_i$, and where $\mathcal{J}(x, \psi^{-1}_x(\widehat{y}) = L(x)^{-1}$ denotes the Jacobian associated with the map in (2) while $\widehat{\gamma}_1$ is the reference fiber for the 2D case. Analogously, we have

$$\begin{aligned} & \|z^b_{\mathbf{m}} - v^{b,h}_{\mathbf{m}}\|^2_{L^2(\zeta^i_t)} \leq \widetilde{C} \sum_{k=1}^{m_i} [(z^i_k - v^{i,h}_k)(x^i_t)]^2 \int_{\widehat{\gamma}_1} \varphi^2_k(\widehat{y}) \left| \mathcal{J}^{-1}(x^i_t, \psi^{-1}_{x^i_t}(\widehat{y}) \right| d\widehat{y} \\ =\ & \widetilde{C} \sum_{k=1}^{m_i} [(z^i_k - v^{i,h}_k)(x^i_t)]^2\, L(x^i_t) \leq \widetilde{C} \sum_{k=1}^{m_i} \max_{x \in K^i_l} L(x)\, [(z^i_k - v^{i,h}_k)(x^i_t)]^2, \end{aligned} \tag{42}$$

with $\widetilde{C}$ the same constant as in (41). From now on $\widetilde{C}$ will be used for a constant whose value can change from line to line.
In the sequel, we choose in (39) $v^{b,h}_{\mathbf{m}} = z^{b,h}_{\mathbf{m}} - I^1(z^b_{\mathbf{m}} - z^{b,h}_{\mathbf{m}})$, with $I^1(\cdot)$ the one-dimensional Clément quasi-interpolant ([14]). Thanks to the Cauchy-Schwarz inequality, we bound the first integral in (40) as

$$\begin{aligned} & \Big| \int_{R^i_l} r_{R^i_l}(u^{b,h}_{\mathbf{m}})\, (z^b_{\mathbf{m}} - v^{b,h}_{\mathbf{m}})\big|_{R^i_l}\, dR^i_l \Big| \leq \|r_{R^i_l}(u^{b,h}_{\mathbf{m}})\|_{L^2(R^i_l)}\, \|z^b_{\mathbf{m}} - v^{b,h}_{\mathbf{m}}\|_{L^2(R^i_l)} \\ & \leq C\, h^i_l\, \|r_{R^i_l}(u^{b,h}_{\mathbf{m}})\|_{L^2(R^i_l)} \left( \max_{x \in K^i_l} L(x) \right)^{1/2} \sum_{k=1}^{m_i} \big| z^i_k - z^{i,h}_k \big|_{H^1(\widetilde{K}^i_l)}, \end{aligned} \tag{43}$$

with $\widetilde{K}^i_l$ defined as in (28), and where we have exploited relation (41) together with the standard estimate associated with $I^1$ to control the $L^2$-norm of the interpolation error.

Let us consider now the second integral in (40). The Cauchy-Schwarz inequality yields

$$\Big| \int_{\partial R^i_l} j_{R^i_l}\, (z^b_{\mathbf{m}} - v^{b,h}_{\mathbf{m}})\big|_{\partial R^i_l}\, d\partial R^i_l \Big| \leq \|j_{R^i_l}\|_{L^2(\partial R^i_l)}\, \|z^b_{\mathbf{m}} - v^{b,h}_{\mathbf{m}}\|_{L^2(\partial R^i_l)}.$$

Norm $\|z^b_{\mathbf{m}} - v^{b,h}_{\mathbf{m}}\|_{L^2(\partial R^i_l)}$ reduces to the sum $\|z^b_{\mathbf{m}} - v^{b,h}_{\mathbf{m}}\|_{L^2(\zeta^i_{l-1})} + \|z^b_{\mathbf{m}} - v^{b,h}_{\mathbf{m}}\|_{L^2(\zeta^i_l)}$ for $l \in \{2, \ldots, n_i - 1\}$, and to the norm $\|z^b_{\mathbf{m}} - v^{b,h}_{\mathbf{m}}\|_{L^2(\zeta^i_1)}$ or $\|z^b_{\mathbf{m}} - v^{b,h}_{\mathbf{m}}\|_{L^2(\zeta^i_{n_i-1})}$ only, for $l = 1$ and $l = n_i$, respectively. Thus, relation (42), employed once or twice according to the value of $l$, and combined with the trace estimate for $L^2$-norm of the interpolation error associated with the quasi-interpolant $I^1$, yields the bound

$$\begin{aligned} &\Big| \int_{\partial R^i_l} j_{R^i_l} \, (z^b_{\mathbf{m}} - v^{b,h}_{\mathbf{m}})\big|_{\partial R^i_l} \, d\partial R^i_l \Big| \\ \leq \;& C \, (h^i_l)^{1/2} \, \|j_{R^i_l}\|_{L^2(\partial R^i_l)} \, \big( \max_{x \in K^i_l} L(x) \big)^{1/2} \sum_{k=1}^{m_i} \big\| z^i_k - z^{i,h}_k \big\|_{H^1(\widetilde{K}^i_l)}. \end{aligned} \tag{44}$$

Finally, we focus on the third integral in (40). Thanks to standard relations between jumps and averages (see, e.g., [3]) and to the orthogonality relation implied by definition (3), we first rewrite the jump term as

$$\begin{aligned} &\big[\partial_\nu u^{b,h}_{\mathbf{m}} (z^b_{\mathbf{m}} - v^{b,h}_{\mathbf{m}})\big]_{\Sigma_j} = \big[\partial_\nu u^{b,h}_{\mathbf{m}}\big]_{\Sigma_j} \big\{ z^b_{\mathbf{m}} - v^{b,h}_{\mathbf{m}} \big\}_{\Sigma_j} + \big\{ \partial_\nu u^{b,h}_{\mathbf{m}} \big\}_{\Sigma_j} \big[ z^b_{\mathbf{m}} - v^{b,h}_{\mathbf{m}} \big]_{\Sigma_j} \\ &= \big[\partial_\nu u^{b,h}_{\mathbf{m}}\big]_{\Sigma_j} \big\{ z^b_{\mathbf{m}} - v^{b,h}_{\mathbf{m}} \big\}_{\Sigma_j} + \big( \big\{ \partial_\nu u^{b,h}_{\mathbf{m}} \big\}_{\Sigma_j} - \mathcal{P}_{\Sigma_j} \big\{ \partial_\nu u^{b,h}_{\mathbf{m}} \big\} \big) \big[ z^b_{\mathbf{m}} - v^{b,h}_{\mathbf{m}} \big]_{\Sigma_j}. \end{aligned}$$

Thus, via the Cauchy-Schwarz inequality, we have

$$\begin{aligned} &\Big| \int_{\Sigma_j} \big[\partial_\nu u^{b,h}_{\mathbf{m}} (z^b_{\mathbf{m}} - v^{b,h}_{\mathbf{m}})\big]_{\Sigma_j} \, d\Sigma_j \Big| \leq \big\| \big[\partial_\nu u^{b,h}_{\mathbf{m}}\big]_{\Sigma_j} \big\|_{L^2(\Sigma_j)} \big\| \big\{ z^b_{\mathbf{m}} - v^{b,h}_{\mathbf{m}} \big\}_{\Sigma_j} \big\|_{L^2(\Sigma_j)} \\ + \;& \big\| \big\{ \partial_\nu u^{b,h}_{\mathbf{m}} \big\}_{\Sigma_j} - \mathcal{P}_{\Sigma_j} \big\{ \partial_\nu u^{b,h}_{\mathbf{m}} \big\} \big\|_{L^2(\Sigma_j)} \big\| \big[ z^b_{\mathbf{m}} - v^{b,h}_{\mathbf{m}} \big]_{\Sigma_j} \big\|_{L^2(\Sigma_j)}. \end{aligned} \tag{45}$$

Now, by mimicking the computations leading to (44) on the average term, we obtain

$$\begin{aligned} &\big\| \big\{ z^b_{\mathbf{m}} - v^{b,h}_{\mathbf{m}} \big\}_{\Sigma_j} \big\|^2_{L^2(\Sigma_j)} \\ \leq \;& C \Big\{ \big\| (z^b_{\mathbf{m}} - v^{b,h}_{\mathbf{m}})\big|_{\Omega_j} \big\|^2_{L^2(\Sigma_j)} + \big\| (z^b_{\mathbf{m}} - v^{b,h}_{\mathbf{m}})\big|_{\Omega_{j+1}} \big\|^2_{L^2(\Sigma_j)} \Big\} \\ \leq \;& C \Big[ \sum_{k=1}^{m_j} \max_{x \in K^j_{n_j}} L(x) \, h^j_{n_j} \big\| z^j_k - z^{j,h}_k \big\|^2_{H^1(\widetilde{K}^j_{n_j})} \\ &+ \sum_{k=1}^{m_{j+1}} \max_{x \in K^{j+1}_1} L(x) \, h^{j+1}_1 \big\| z^{j+1}_k - z^{j+1,h}_k \big\|^2_{H^1(\widetilde{K}^{j+1}_1)} \Big], \end{aligned}$$

with $C = C(m_j, m_{j+1})$. An analogous estimate can be derived for the jump contribution $\big\| \big[ z^b_{\mathbf{m}} - v^{b,h}_{\mathbf{m}} \big]_{\Sigma_j} \big\|_{L^2(\Sigma_j)}$ in (45), so that we can bound the integral on $\Sigma_j$ in (40):

$$\begin{aligned} &\Big| \int_{\Sigma_j} \big[\partial_\nu u^{b,h}_{\mathbf{m}} (z^b_{\mathbf{m}} - z^{b,h}_{\mathbf{m}})\big]_{\Sigma_j} \, d\Sigma_j \Big| \\ \leq \;& C \Big[ \big\| \big[\partial_\nu u^{b,h}_{\mathbf{m}}\big]_{\Sigma_j} \big\|_{L^2(\Sigma_j)} + \big\| \big\{ \partial_\nu u^{b,h}_{\mathbf{m}} \big\}_{\Sigma_j} - \mathcal{P}_{\Sigma_j} \big\{ \partial_\nu u^{b,h}_{\mathbf{m}} \big\} \big\|_{L^2(\Sigma_j)} \Big] \\ &\Big[ (h^j_{n_j})^{1/2} \big( \max_{x \in K^j_{n_j}} L(x) \big)^{1/2} \sum_{k=1}^{m_j} \big\| z^j_k - z^{j,h}_k \big\|_{H^1(\widetilde{K}^j_{n_j})} \\ &+ (h^{j+1}_1)^{1/2} \big( \max_{x \in K^{j+1}_1} L(x) \big)^{1/2} \sum_{k=1}^{m_{j+1}} \big\| z^{j+1}_k - z^{j+1,h}_k \big\|_{H^1(\widetilde{K}^{j+1}_1)} \Big]. \end{aligned} \tag{46}$$

In view of definitions (30)-(38) estimate (29) now promptly follows by applying inequalities (43), (44) and (46) to (40). □

By exploiting estimate (29) to make computable the discretization contribution in (20), we identify as the actual *a posteriori* estimator for the global functional error $|J(e^{b,h}_{\mathbf{m}})|$ the quantity

$$\eta^{b,h}_{\mathbf{mm}^+} = \eta^{b}_{\mathbf{mm}^+} + \eta^{h}_{\mathbf{mm}^+}, \tag{47}$$

with $\eta^{b}_{\mathbf{mm}^+}$ the a posteriori modeling error estimator and

$$\eta^{h}_{\mathbf{mm}^+} = \eta_h + \eta_{NCF} + \eta_{NC} \tag{48}$$

the a posteriori error estimator for the discretization error.
All the three contributions in (48) share the structure typical of a goal-oriented analysis since coinciding with the product of a residual depending on the primal problem and a weight depending on the dual problem. In more detail, the fiber structure characterizing the Hi-Mod reduction procedure leads to a peculiar definition for the weights where the contribution along the $x$- and $\mathbf{y}$-directions remains separate.
Of course, to make computable the estimator $\eta^{h}_{\mathbf{mm}^+}$ we have to replace the (unknown) dual solution $z^{b}_{\mathbf{m}}$ with a suitable discrete counterpart. In particular, we resort to the discrete enriched dual solution $z^{b,h}_{\mathbf{m}^+}$.

**Remark 4.2** *Estimator* (29) *can be extended to more general boundary conditions on* $\partial\Omega$*, provided that the definition of the boundary residual* $j_{R^i_l}$ *is modified accordingly. A generalization of* (29) *to a 3D framework is also possible with a proper choice of the map* $\psi_x$*. Indeed, the orthonormality of the modal basis can be exploited in* (43) *and* (44) *only if* $\mathcal{J}^{-1}(x, \psi_x^{-1}(\widehat{\mathbf{y}}))$ *does not depend on* $\widehat{\mathbf{y}}$*. This is always guaranteed in a 2D setting while it has to be explicitly required in a 3D framework.*

## 4.2 The m$h$-adaptive procedure

Moving from the estimator $\eta^{b,h}_{\mathbf{mm}^+}$, the ultimate goal of this work is to provide an effective way to automatically select the macro-partition $\mathcal{T}_\Omega$ of $\Omega$ with the corresponding modal multi-index $\mathbf{m}$ as well as the finite element subdivision $\mathcal{T}^i_h = \{K^i_l\}_{l=1}^{n_i}$ of $\Omega_{1D,i}$ with $i \in \{1, \dots, s\}$. In more detail, with this choice we aim at estimating the global functional error $|J(u) - J(u^{b,h}_{\mathbf{m}})|$ within a fixed (global) tolerance `TOL`.

The crucial issue is how to combine the model with the mesh adaptivity. Different strategies are proposed in the literature to balance the two sources of error (see, e.g., [2, 10, 25]). The approach we follow here iteratively alternates model with mesh adaptivity until the desired accuracy on $|J(u) - J(u^{b,h}_{\mathbf{m}})|$ is achieved. We stress again that the structure of the estimator $\eta^{b,h}_{\mathbf{mm}^+}$ specifically fits for this

purpose since the model and the mesh error contributions are separated.
The **m**-adaptive phase corresponds to the same procedure detailed in Section 3.2. Concerning the $h$-adaptive phase, it is anticipated to be a straightforward step since the finite element discretization is applied to a one-dimensional domain. At the beginning of the $h$-adaptive phase, the partition $\mathcal{T}_\Omega$ and the modal multi-index $\mathbf{m}$ are fixed, while the finite element partition $\{\mathcal{T}_h^i\}$ is uniform on each $\Omega_{1D,i}$ for $i \in \{1,\dots,s\}$. The goal is to adapt the distribution of the finite element nodes along $\Omega_{1D}$ to fit the solution dynamics along the mainstream and to guarantee the fulfillment of a given tolerance `TOLH` on the functional discrete error. As usual, the finite element mesh is updated via an error equidistribution criterion on the subintervals $K_l^i$, i.e., we demand that $\eta_{\mathbf{mm}^+}^{h,i,l} = \texttt{TOLH}/N_h$ for $l \in \{1,\dots,n_i\}$ and $i \in \{1,\dots,s\}$ (see lines `8.` and `10.` in the subsequent pseudo-code), where $\eta_{\mathbf{mm}^+}^{h,i,l} = \eta_{\mathbf{mm}^+}^h\big|_{R_l^i}$ denotes the discretization error estimator associated with $R_l^i$, while $N_h$ stands for the cardinality of the current finite element mesh $\{\mathcal{T}_h^i\}_{i=1}^s$ on $\Omega_{1D}$.
The main steps of the $h$-adaptive procedure are here coded:

```
1.  set k=0;
2.  compute η^h_mm+ via (48);
3.  while( η^h_mm+ > TOLH & k < NmaxH ) {
    4.  for i=1:s
        5.  for l=1:n_i
            6.  compute η^{h,i,l}_mm+ ;
            7.  if η^{h,i,l}_mm+ > deltaH1 TOLH/N^k_h
                8.  bisect K^i_l;
            9.  elseif max(η^{h,i,l}_mm+, η^{h,i,l-1}_mm+) < deltaH2 TOLH/N^k_h & l>1
                10.  merge K^i_l and K^i_{l-1};
                end
            end
        end
    11.  k=k+1;
    12.  compute η^h_mm+ via (48); }
```

A maximal number `NmaxH` of iterations is allowed, while $\texttt{N}_h^{\texttt{k}}$ denotes the cardinality of the `k`-th adapted grid. As usual, the mesh coarsening is a more difficult task with respect to mesh refinement: the local error estimator associated with at least two consecutive subintervals has to be sufficiently small before glueing the subintervals (line `10.` of the pseudo-code). The parameters `deltaH1` and `deltaH2` limit the mesh refinement and coarsening to "the worst" and "the best" subintervals, respectively.

Loop at line `3.` is entered only if the model predicted by the **m**-adaptive procedure discretized on the initial uniform mesh does not ensure the desired accuracy. We highlight that the evaluation of the error estimator at step `12.` requires a projection of the reduced solutions $u_{\mathbf{m}}^{b,h}$, $z_{\mathbf{m}}^{b,h}$, $z_{\mathbf{m}^+}^{b,h}$ on the new mesh.

The final output of the $h$-adaptive procedure is a new finite element partition of $\Omega_{1D}$ given by the union $\cup_{i=1}^{s}\widetilde{\mathcal{T}}_h^i$, where $\widetilde{\mathcal{T}}_h^i = \{\widetilde{K}_l^i\}_{l=1}^{\widetilde{n}_i}$ denotes the adapted partition predicted for the subinterval $\Omega_{1D,i}$. The lenght of the adapted intervals $\widetilde{K}_l^i$ can now vary along $\Omega_{1D,i}$ as well as the number $\widetilde{n}_i$ of intervals may change from subdomain to subdomain.

Now we are ready to set up the whole **m**$h$-adaptive procedure. We denote by `TOL` the global tolerance demanded on the global error $|J(u) - J(u_{\mathbf{m}}^{b,h})|$. The idea of separately dealing with model and mesh adaptivity suggests us to define two distinct tolerances to adapt independently the model and the mesh. For this purpose, we set `TOLM` $= \theta$ `TOL` and `TOLH` $= (1-\theta)$ `TOL` with $0 \leq \theta \leq 1$. The value $\theta$ establishes a ratio between modeling and discretization error, in agreement with what stated in Remark 4.1.
The **m**$h$-adaptive procedure can be listed as follows:

`1.` set k=0;
`2.` compute $\eta_{\mathbf{mm}^+}^{b,h}$ via (47);
`3.` if $\eta_{\mathbf{mm}^+}^{b,h} \leq$ TOL, break;
`4.` while( $\eta_{\mathbf{mm}^+}^{b,h} >$ TOL & k < Nmax ) {
`6.` **m**-adaptive procedure;
`7.` $h$-adaptive procedure;
`8.` k=k+1;
`9.` compute $\eta_{\mathbf{mm}^+}^{b,h}$ via (47);
`10.` if $\eta_{\mathbf{mm}^+}^{b,h} \leq$ TOL, break; }

A maximum number `Nmax` of iterations guarantees the end of the **m**$h$-adaptive procedure. Again we point out that a projection on the updated mesh of the reduced solutions involved in the estimators is required before each new iteration of the whole procedure.

### 4.3 Numerical assessment of the m$h$-adaptive procedure

This section presents two test cases. The first test is essentially meant to assess the **m**$h$-adaptive procedure from a qualitative viewpoint: in particular, we analyze the sensitivity of the predicted model and discretization with respect to the chosen goal functional. The second case focuses on a configuration of some interest in hydrodynamics.

For both the test cases, we show that one single iteration of the **m**$h$-adaptive procedure suffices.

### 4.3.1 Test case: diffusion heterogeneity

We solve the pure diffusive problem $-\nabla \cdot (\mu \nabla u) = f$, completed with full homogeneous Dirichlet boundary conditions, on the trapezoidal domain $\Omega$ bounded, counterclockwise, by the straight lines $x = 0$, for $0 \leq y \leq 1$; $y = -0.1x$, for $0 \leq x \leq 4$; $x = 4$, for $-0.4 \leq y \leq 1.4$; $y = 1 + 0.1x$, for $0 \leq x \leq 4$. In particular, the viscous coefficient $\mu$ coincides with the Gaussian function $1 + 100 \exp(-[(x-1)^2 + (y-0.32)^2]/0.05)$, while the source term is set to one. Figure 7 shows the corresponding full solution computed on a uniform unstructured grid of about 110000 triangles. The shape of the contour plots highlights the localized nature of the viscous coefficient.

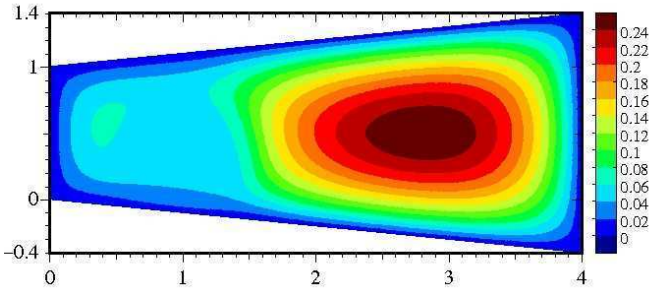


Figure 7: Full solution $u$

We run the $\mathbf{m}h$-adaptive procedure with two different choices for the functional of interest $J$. We control first a global and then a local quantity, the last task being, in general, more challenging. In more detail, we pick $J_1(v) = [\text{meas}(\Omega)]^{-1} \int_\Omega v(x,y)\, d\mathbf{z}$ and $J_2(v) = [\text{meas}(\varpi)]^{-1} \int_\varpi v(x,y)\, d\mathbf{z}$ with $v \in L^1(\Omega)$, to control the mean value of the solution on the whole domain $\Omega$ and on the region $\varpi = \Omega \cap \{(x,y) : x < 1.5\}$, respectively.

We make the same choice for the input parameters of the $\mathbf{m}h$-adaptive procedure for both the functionals. Concerning the modeling phase, we select $\widetilde{m} = 1$, $\widetilde{m}^+ = 3$; $\phi = 0.16$; $\delta = 1$; `deltaM1` $= 0.5$; `deltaM2` $= 1.5$; `NmaxM` $= 8$; then, a uniform finite element partition of size $h = 0.2$ is introduced on $\Omega_{1D} = (0,4)$. As far as the mesh adaptivity is concerned, the parameters `deltaH1` and `deltaH2` are set to 0.5 and 1.5, respectively while the maximum number `NmaxH` of iterations is fixed to 15. Notice that the initial mesh is selected to be significantly coarse. Finally, we choose a global tolerance `TOL` $= 0.1$, the parameter $\theta = 0.05$ and a maximum number `Nmax`$= 10$ of $\mathbf{m}h$-adaptive iterations.
For the sake of simplicity, we do not perform any calibration of the saturation constant $\beta_{\mathbf{m}}$ in (12), simply by setting $\beta_{\mathbf{m}} = 0$ in (13).

For both the functionals the $\mathbf{m}$-adaptive procedure identifies three subdomains: for $J = J_1$ we get $\Omega_1 = (0, 0.6) \times (-0.4, 1.4) \cap \Omega$, $\Omega_2 = (0.6, 1.8) \times (-0.4, 1.4) \cap \Omega$, $\Omega_3 = (1.8, 4) \times (-0.4, 1.4) \cap \Omega$; for $J = J_2$ we obtain $\Omega_1 = (0, 0.6) \times$

$(-0.4, 1.4) \cap \Omega$, $\Omega_2 = (0.6, 1.6) \times (-0.4, 1.4) \cap \Omega$, $\Omega_3 = (1.6, 4) \times (-0.4, 1.4) \cap \Omega$. The modal multi-indices predicted as initial guess for the **m**-adaptive phase are $\mathbf{m}^{(0)} = \{1, 2, 1\}$ and $\mathbf{m}^{+\,(0)} = \{3, 4, 3\}$ for both the goal functionals. A tolerance of $10^{-3}$ is set in the domain decomposition algorithm at both the interfaces.
A single iteration suffices to achieve the accuracy `TOLM` for both the choices of $J$ and the final prediction for the modal multi-index is $\mathbf{m} = \mathbf{m}^{(1)} = \{1, 3, 1\}$ in both the cases. As expected, the largest number of modes is employed in $\Omega_2$, i.e., where the significant transverse dynamics take place. Notice that the global nature of the control via $J_1$ reflects into the selection of a domain $\Omega_2$ which is slightly wider than for $J_2$. Figure 8 shows the piecewise hierarchically reduced

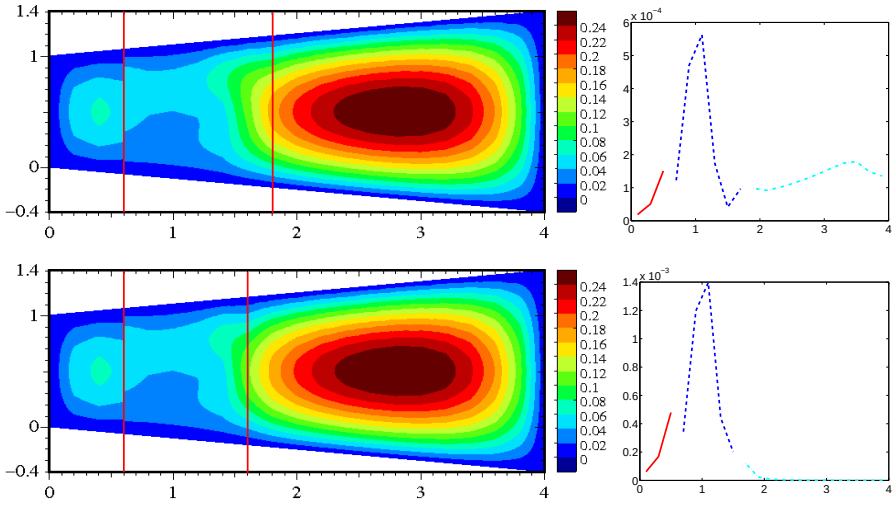


Figure 8: Piecewise hierarchically reduced solution and distribution of the corresponding estimator for $\mathbf{m} = \{1, 3, 1\}$, $\mathbf{m}^+ = \{3, 5, 3\}$ and for the control of $J_1$ (top) and $J_2$ (bottom)

solution predicted by the **m**-adaptive procedure for $J_1$ (top) and $J_2$ (bottom) together with the distribution of the corresponding error estimator (the three different colors correspond to the modeling error estimators $\eta^{b,i}_{\mathbf{mm}^+}$ associated with the subdomains $\Omega_i$ for $i \in \{1, \ldots, 3\}$). The control of the mean value leads to a reduced solution which is very similar to the full one. The coarseness of the finite element mesh motivates the irregular contour lines in Figure 8, especially in $\Omega_1$ and $\Omega_2$ where the solution exhibits an irregular trend along the horizontal direction. Finally, in accordance with the conformity analysis in [31], the model discontinuity is more evident along $\Sigma_1 = \{0.6\} \times \gamma_{0.6}$ since $m_1 < m_2$.

The $h$-adaptive procedure converges after three iterations for both the choices of $J$. We show in Figure 9 the corresponding adapted meshes which consist of 47 and 62 elements, respectively. The two meshes exhibit a distinct distribution of the subintervals which matches the selected goal-functional. As expected, the

control of $J_2$ locates most of the nodes in the left part of $\Omega_{1D}$: the control of the global mean value predicts 29 subintervals on $(0, 1.8)$ while 50 subintervals are predicted on $(0, 1.6)$ when $J = J_2$. These results confirm the sensitivity of the $h$-adaptive (and consequently of the $\mathbf{m}h$-adaptive) procedure with respect to the selected $J$.

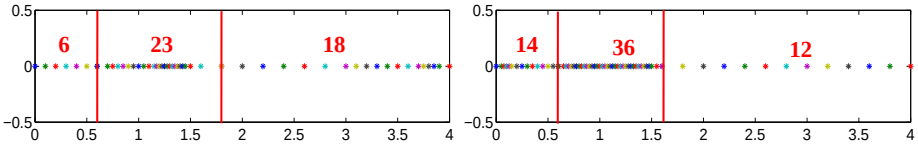


Figure 9: Adapted meshes associated with $J_1$ (left) and $J_2$ (right); the numbers refer to the number of intervals on each $\Omega_{1D,i}$

### 4.3.2 Third test case

We model the water dynamics in a straight channel $\Omega = (0, 10) \times (0, 1.5)$ whose bed is restricted by a pier. In particular, to guarantee the regularity demanded for the map $\Psi$ in Section 2, we approximate the shape of the pier with a gaussian profile (see Fig. 10 (top)). We solve the advection-diffusion problem

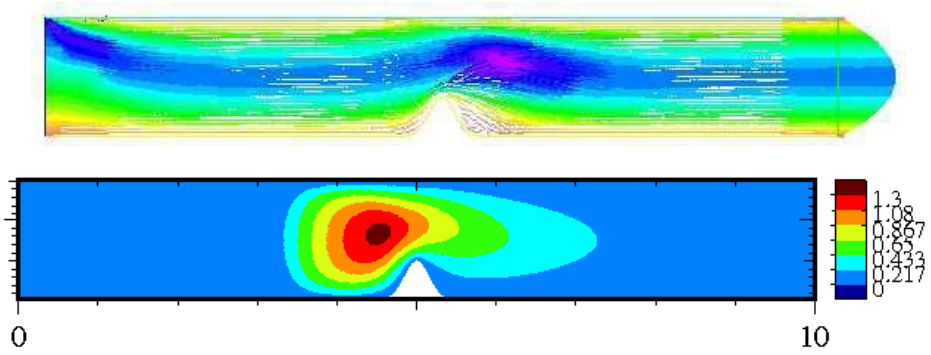


Figure 10: Domain $\Omega$ and advective field $\mathbf{b}$ (top); full solution $u$ (bottom)

$-\mu\Delta u + \mathbf{b}\cdot\nabla u = f$, with $\mu = 0.1$, $f(x, y) = (x-4)^2 + (y-0.75)^2 < 0.5$, while $\mathbf{b}$ is the velocity field in Fig. 10 (top). The advection-diffusion problem is completed by full homogeneous Dirichlet boundary conditions. As reference model, we are interested in the dynamics of pollutant flowing in the channel $\Omega$; more precisely, we aim at controlling the mean value of the concentration $u$ of pollutant over the whole domain. We set therefore $J(v) = \int_\Omega v(x, y)\, d\mathbf{z}$, for $v \in L^1(\Omega)$. In Fig. 10 (bottom) we show the contour plots of the full solution approximated on a uniform unstructured mesh of about 18000 elements. The picture clearly

shows how the contour lines are affected by the presence of the pier.
We stress that the analysis below is far from any quantitative interpretation of the pollutant convection; it has to be meant just as an academic test case to assess the **m**$h$-adaptive procedure on a configuration of some interest in hydrodynamics.

We run the **m**$h$-adaptive procedure with the following input parameters. For the modeling phase, we choose $\widetilde{m} = 1$, $\widetilde{m}^+ = 3$, $\phi = 0.1$, $\delta = 1$, `deltaM1` $= 0.5$, `deltaM2` $= 1.5$, `NmaxM` $= 10$ and a uniform finite element partition of size $h = 0.2$ to discretize $\Omega_{1D} = (0, 10)$. The mesh adaptivity is set with `deltaH1` $= 0.5$, `deltaH2` $= 1.5$, `NmaxH`$= 15$. Finally, we fix a global tolerance `TOL` $= 5$, the parameter $\theta = 0.0018$, `Nmax`$= 10$ and the saturation constant $\beta_{\mathbf{m}} = 0$.

The **m**-adaptive procedure detects the three subdomains $\Omega_1 = (0, 4.6) \times (0, 1.5)$, $\Omega_2 = (4.6, 5.2) \times (0, 1.5)$ and $\Omega_3 = (5.2, 10) \times (0, 1.5)$. The reduced extension of $\Omega_2$ essentially suggests that the thresholding procedure identifies the area around the pier as the most troublesome for the control of $J$. The initial guess predicted for the modal multi-indices are $\mathbf{m}^{(0)} = \{1, 2, 1\}$, $\mathbf{m}^{+\,(0)} = \{3, 4, 3\}$. As far as the domain decomposition algorithm is concerned, the presence of the advective field **b** immediately raises an important issue with respect to the well-posedness of both the primal and the dual problems. We have to properly select the Dirichlet and the Neumann interface according to the field direction. Thus, a Neumann/Dirichlet condition is assigned at $\Sigma_1 = \{4.6\} \times \gamma_{4.6}$ and $\Sigma_2 = \{5.2\} \times \gamma_{5.2}$ when solving the primal problem; conversely, a Dichlet/Neumann condition is enforced for the dual problem. We fix a tolerance equal to $10^{-2}$ for the domain decomposition algorithm at both $\Sigma_1$ and $\Sigma_2$. At this stage the average number of iterations to guarantee the desired accuracy is nine.
Two model adaptivity iterations are enough to reach the tolerance `TOLM`, with a final prediction for the modal multi-index $\mathbf{m} = \mathbf{m}^{(2)} = \{3, 2, 3\}$. To control $J$, an additional mode is employed where the pollutant is released as well as in the wake area, behind the pier.

The $h$-adaptive procedure converges at the fourth iteration. During the first three iterations the mesh is preserved uniform on both $\Omega_{1D,1}$ and $\Omega_{1D,3}$, while it is gradually refined on $\Omega_{1D,2}$ (the number of nodes increases from 7 to 24). At the last iteration, only a coarsening of the mesh on $\Omega_{1D,1}$ occurs (notice that the first internal node coicides with 3). Figure 12 (left) shows the four adapted meshes together with a corresponding zoom in on $\Omega_{1D,2}$ (right) to highlight the crowding of the nodes in the area around the pier.
In Figure 11 we show the piecewise hierarchically reduced primal (top) and dual (bottom) solutions computed on the last adapted mesh. As expected, the control of the mean value leads to a reduced primal solution similar to the full one (compare Fig. 10 (bottom) with Fig. 11 (top)). Moreover, since the goal quantity is distributed on $\Omega$, the dual problem identifies the whole domain as influencing the functional $J$. Finally, in Figure 11 (middle) we show the reduced dual solution computed on the third adapted grid. Notice that the dual solution

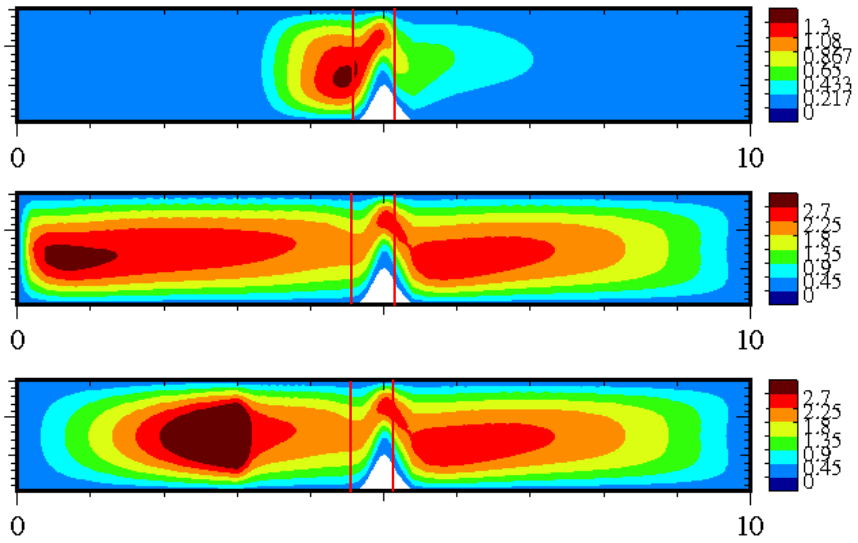


Figure 11: Piecewise hierarchically reduced solutions for $\mathbf{m} = \{3, 2, 3\}$: primal (top) and dual (bottom) solution on the last adapted mesh; dual solution on the third adapted mesh (middle)

on the last mesh overestimates the size of the boundary layer along $\Gamma_0$ because of the the coarseness of the finite element mesh in the first part of $\Omega_{1D,1}$.

## 5 Future developments

Possible extensions of the Hi-Mod reduction include the generalization of our approach to time-dependent and nonlinear problems. Moreover, in view of practical problems, we plan to implement the proposed approach in a 3D setting. Different modal bases (see [29] for a first example in such a direction) as well as coupling algorithms alternative to the Dirichlet/Neumann scheme represent also topics of some interest.

## Acknowledgements

The authors wish to thank warmly Alexandre Ern for many discussions and fundamental suggestions he gave along the entire preparation of the manuscript.

## References

[1] Achchab, B., Achchab, S., Agouzal, A.: Some remarks about the hierarchical a posteriori error estimate. Numer. Methods Partial Differential Equations

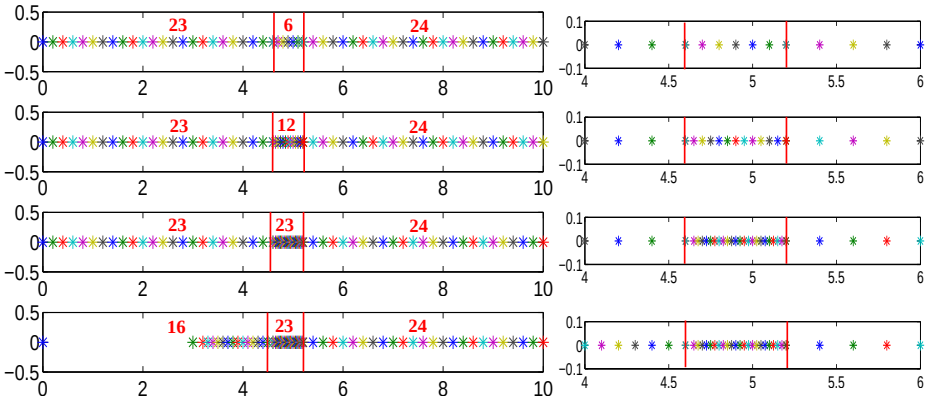


Figure 12: Whole adapted mesh (left) and zoom in on the area with the pier (right) at the different adaptive iterations (top-bottom); the numbers refer to the number of intervals on each $\Omega_{1D,i}$

**20**(6), 919–932 (2004)

[2] Ainsworth, M.: A posteriori error estimation for fully discrete hierarchic models of elliptic boundary value problems on thin domains. Numer. Math. **80**, 325–362 (1998)

[3] Arnold, D.N., Brezzi, F., Cockburn, B., Marini, L.D.: Unified analysis of discontinuous Galerkin methods for elliptic problems. SIAM J. Numer. Anal. **39**, 1749–1779 (2002)

[4] Bangerth, W., Rannacher, R.: Adaptive Finite Element Methods for Differential Equations. Birkhauser Verlag, Basel (2003)

[5] Bank, R.E., Smith, R.K.: A posteriori error estimates based on hierarchical bases. SIAM J. Numer. Anal. **30**, 921–935 (1993)

[6] Bank, R.E., Weiser, A.: Some a posteriori error estimators for elliptic partial differential equations. Math. Comp. **44**, 285–301 (1985)

[7] Becker, R., Rannacher, R.: An optimal control approach to a posteriori error estimation in finite element methods. Acta Numer. **10**, 1–102 (2001)

[8] Bernardi, C., Maday, Y., Patera, A.T.: Domain decomposition by the mortar element method. NATO Adv. Sci. Inst. Ser. C Math. Phys. Sci. **384**, Kluwer Acad. Publ., Dordrecht (1993)

[9] Blanco, P.J., Leiva, J.S., Feijóo, R.A., Buscaglia, G.C.: Black-box decomposition approach for computational hemodynamics: one-dimensional models. Comput. Methods Appl. Mech. Eng. **200**(13-16), 1389–1405 (2011)

[10] Braack, M., Ern, A.: A posteriori control of modeling errors and discretization errors. Multiscale Model Simul. **1**, 221–238 (2003)

[11] Bruckstein, A.M., Donoho, D.L., Elad, M.: From sparse solutions of systems of equations to sparse modeling of signal and images. SIAM Review **51**(1), 34–81 (2009)

[12] Cardiovascular Mathematics, Modeling and Simulation of the Circulatory System. In: Formaggia, L., Quarteroni, A., Veneziani, A. (eds.), Modeling Simulation and Applications **1**, Springer, Milano (2009)

[13] Ciarlet, Ph.: The Finite Element Method for Elliptic Problems. North-Holland Publishing Company, Amsterdam (1978)

[14] Clément, Ph.: Approximation by finite element functions using local regularization. RAIRO Anal. Numer. **2**, 77–84 (1975)

[15] Dörfler, W., Nochetto, R.H.: Small data oscillation implies the saturation assumption. Numer. Math. **91**, 1–12 (2002)

[16] Ern, A., Perotto, S., Veneziani, A.: Hierarchical model reduction for advection-diffusion-reaction problems. In: K. Kunisch, G. Of and O. Steinbach, eds., Numerical Mathematics and Advanced Applications, Springer-Verlag, Berlin Heidelberg, pp. 703–710 (2008)

[17] Formaggia, L., Nobile, F., Quarteroni, A., Veneziani, A.: Multiscale modelling of the circulatory system: a preliminary analysis. Comput. Visual. Sci. **2**, 75–83 (1999)

[18] Giles, M.B., Süli, E.: Adjoint methods for PDEs: a posteriori error analysis and postprocessing by duality. Acta Numer. **11**, 145–236 (2002)

[19] Hinze, M., Volkwein, S.: Proper orthogonal decomposition surrogate models for nonlinear dynamical systems: error estimates and suboptimal control. Dimension reduction of large-scale systems. Lect. Notes Comput. Sci. Eng. **45**, Springer, Berlin, pp. 261-306 (2005)

[20] Johnson, C.: A new paradigm for adaptive finite element methods. In: Proceedings of MAFELAP 93, John Wiley, J. Whiteman, eds., (1993)

[21] Lacour, C., Maday, Y.: Two different approaches for matching nonconforming grids: the mortar element method and the FETI method. BIT, **37**, 720–738 (1997)

[22] Lasis, A., Süli, E.: Poincaré-type inequalities for broken Sobolev spaces. Tech. Report 03-10, Oxford University Computing Laboratory (2003)

[23] Lions, J.L., Magenes, E.: Non Homogeneous Boundary Value Problems and Applications. Springer, Berlin-Heidelberg-New York (1972)

[24] Maday, Y., Ronquist, E.M.: A reduced-basis element method. C. R. Acad. Sci. Paris Ser. **I**(335), 195–200 (2002)

[25] Micheletti, S., Perotto, S., David, F.: Model adaptation enriched with an anisotropic mesh spacing for nonlinear equations: application to environmental and CFD problems. To appear in Numer. Math. Theor. Meth. Appl. (2013)

[26] Miglio, E., Perotto, S., Saleri, F.: Model coupling techniques for free-surface flow problems. Part I. Nonlinear Analysis **63**, 1885–1896 (2005)

[27] Multiscale wavelet methods for partial differential equations. In: Dahmen, W., Kurdila, A.J., Oswald, P. (eds.), Wavelet Analysis and its Applications **6**, Academic Press, Inc., San Diego (1997)

[28] Oden, J.T., Prudhomme, S.: Goal-oriented error estimation and adaptivity for the finite element method. Comput. Math. Appl. **41**, 735–756 (2001)

[29] Ohlberger, M., Smetana, K.: A new problem adapted hierarchical model reduction technique based on reduced basis methods and dimensional splitting. Tech. Report 03-10, University Muenster (2010)

[30] Perotto, S.: Hierarchical model (Hi-Mod) reduction in non-rectilinear domains. Accepted for the publication in Proceedings of the 21st International Conference on Domain Decomposition Methods, Springer (2013)

[31] Perotto, S., Ern, A., Veneziani, A.: Hierarchical local model reduction for elliptic problems: a domain decomposition approach. Multiscale Model. Simul. **8**(4), 1102–1127 (2010)

[32] Quarteroni, A., Valli, A.: Domain Decomposition Methods for Partial Differential Equations. Numerical Mathematics and Scientific Computation. Oxford University Press, New York (1999)

[33] Robertson, A.M., Sequeira, A.: A director theory approach for modeling blood flow in the arterial system: an alternative to classical 1D models. Math. Models Methods Appl. Sci. **15**(6), 871–906 (2005)

[34] Toselli, A., Widlund, O.: Domain Decomposition Methods–Algorithms and Theory. Springer-Verlag, Berlin Heidelberg (2005)

# MOX Technical Reports, last issues

**Dipartimento di Matematica "F. Brioschi",**
**Politecnico di Milano, Via Bonardi 9 - 20133 Milano (Italy)**

**20/2013** Azzimonti, L.; Nobile, F.; Sangalli, L.M.; Secchi, P.
*Mixed Finite Elements for spatial regression with PDE penalization*

**21/2013** Perotto, S.; Veneziani, A.
*Coupled model and grid adaptivity in hierarchical reduction of elliptic problems*

**19/2013** Azzimonti, L.; Sangalli, L.M.; Secchi, P.; Domanin, M.; Nobile, F.
*Blood flow velocity field estimation via spatial regression with PDE penalization*

**18/2013** Discacciati, M.; Gervasio, P.; Quarteroni, A.
*Interface Control Domain Decomposition (ICDD) Methods for Coupled Diffusion and Advection-Diffusion Problems*

**17/2013** Chen, P.; Quarteroni, A.
*Accurate and efficient evaluation of failure probability for partial different equations with random input data*

**16/2013** Faggiano, E. ; Lorenzi, T. ; Quarteroni, A.
*Metal Artifact Reduction in Computed Tomography Images by Variational Inpainting Methods*

**15/2013** Antonietti, P.F.; Giani, S.; Houston, P.
*Domain Decomposition Preconditioners for Discontinuous Galerkin Methods for Elliptic Problems on Complicated Domains*

**14/2013** Gianni Arioli, Filippo Gazzola
*A new mathematical explanation of the Tacoma Narrows Bridge collapse*

**13/2013** Pini, A.; Vantini, S.
*The Interval Testing Procedure: Inference for Functional Data Controlling the Family Wise Error Rate on Intervals.*

**12/2013** Antonietti, P.F.; Beirao da Veiga, L.; Bigoni, N.; Verani, M.
*Mimetic finite differences for nonlinear and control problems*